JOURNAL OF COMPUTATIONAL PHYSICS **126,** 181–201 (1996)
ARTICLE NO. 0129

Entropy Controlled Adaptive Finite Element Simulations for Compressible Gas Flow

K. BANAŚ* AND L. DEMKOWICZ†

Section of Applied Mathematics, Cracow University of Technology, 31-155 Kraków, Warszawska 24, Poland; †The Texas Institute for Computational and Applied Mathematics, The University of Texas at Austin, Taylor Hall 2.400, Austin, Texas 78712

Received October 17, 1995; revised December 26, 1995

The principal idea of the present work consists in using the entropy balance equation in its discrete form as a rationale for controling an optimal amount of artifficial dissipation in Finite Element (FE) compressible gas simulations. The entropy control can be reinterpreted as a nonlinear stability estimate in terms of the so-called modified entropy function. The idea has been practically verified using the Taylor-Galerkin method combined with an artificial viscosity term proposed by Hughes and Johnson, in context of *h*-adaptive linear finite elements. The obtained numerical results confirm that the entropy control may indeed provide a basis for the careful balance between stability and higher-order resolution in FE approximations.

1. INTRODUCTION

The vast majority of numerical simulations and related theoretical research in computational fluid dynamics (CFD) has been, until recent years, carried out within the framework of finite difference (FD) and finite volume (FV) methods. Some important proofs on the existence of solutions to the gas dynamics equations have used sequences of approximate FD solutions [1, 2].

The usual approach to ensure the stability of approximate solutions in FD and related FV multidimensional flow simulations consists in constructing a stable algorithm for one-dimensional scalar problems and then formally generalizing it to the vector multidimensional case (even though such a procedure may frequently result in a loss of accuracy [3]). The classical stability criteria for approximate solutions of one-dimensional scalar problems are the maximum principle, the monotonicity property [2, 4], and the total variation diminishing (TVD) property [5]. We emphasize that all these stability criteria are met by the exact solutions to the problem. Based on these properties, several numerical schemes were designed or modified and successfully used in CFD (to reference only a few—[6–10]).

The main drawback of the FD schemes remains the necessity to use highly structured meshes, leading to severe practical difficulties when complicated geometries of flow domains are considered [11]. Also the application of adaptive techniques is complicated and only recently such procedures have been successfully used in FD computations [12].

Finite Element Schemes for Compressible Gas Flow

The main advantage of the FE procedures is the ease of treating the problems defined in domains with complex geometry by means of unstructured grids [13], keeping as the only requirement the continuity of approximate solutions.

The early FE schemes were constructed by adopting classical FD techniques such as artificial viscosity or flux corrected transport [14, 15]. However, the global character of the FE method, related directly to the variational principles, does not allow for a straightforward generalization and application of the stability criteria developed for the one-dimensional FD methods, and, for that reason, these early FE schemes still lack a rigorous stability and convergence analysis.

The mathematical structure of first-order hyperbolic problems (e.g., the Euler equations) and convection dominated, parabolic, or incomplete parabolic problems (e.g., the Navier–Stokes equations) is not well suited for a straightforward application of the (Bubnov-) Galerkin method laying down the foundation for FE approximations. One of the most successful approaches to overcome this difficulty is the SUPG (streamline upwind Petrov Galerkin) method [16], known also as the SD (streamline diffusion) method [17], or in another, strongly related version, as the GLS (Galerkin least squares) method [18]. The idea behind the method is to add to the original first-order operator some (mesh dependent) second-order terms, consistent with the original equations (i.e., not altering the exact solution), which improve the stability properties of the discrete operator. Still, for nonlinear problems yielding discontinuous solutions (shocks), extra nonlinear artificial viscosity (the so-called ''shock capturing operator'') must be added to guarantee stable approximations.

The SUPG and related methods are valid for unstruc-

0021-9991/96 $18.00

tured grids and constitute a significant departure from the classical FD-type approaches. Several proofs of stability and convergence for simplified, model problems have been established (see [17] and the references therein).

Second-order terms of a different kind are added in another computationally popular approach, the Taylor–Galerkin (TG) method [19–21]. Here, the terms are derived from the time discretization analysis and guarantee the second-order accuracy of time approximations (see [22] for some recent generalizations). The added terms play an important double role in establishing both stability in time and stability in space for Galerkin approximations (see [23] for the time stability analysis).

Also in this case, an extra nonlinear artificial viscosity has to be added for problems with discontinuous solutions. Other FE-related concepts include time-splitting procedures combined frequently with the method of characteristics to resolve the transport phenomena [24–26].

Adaptive Finite Element Methods

Probably the most important implication of the use of unstructured grids in finite element space discretization procedures is the straightforward implementation of adaptive techniques where the finite element mesh is reconstructed during the solution procedure to achieve the best possible accuracy with the minimal computational cost [27–29]. The capabilities offered by the adaptive procedures were early recognized [30, 21], and intensive investigations in the area have continued for the last decade [31]. Two main techniques are the *h*-refinement-derefinement algorithm [32, 33], consisting in dividing elements or reconstructing them back, depending upon the error of the actual solution, and the remeshing technique [34], where new grids are constructed, to adapt to the current solution. The general *h-p* adaptive procedures with variable order of approximating polynomials in different elements have also been investigated [21, 35, 36, 25, 23].

Stability of Transient Simulations

The question of stability of solutions to the initial-boundary value problems in gas dynamics has been addressed in [37–40]. Through the use of *linearization* and *localization principles*, the study on stability is reduced to the investigation of related initial-boundary value problems for linear, constant coefficients, incomplete parabolic equations. Fundamental results concerning the number and form of stable boundary conditions, especially those corresponding to open boundaries, have been obtained (see [25, 23] for their FE implementation).

A slightly different philosophy lies behind the derivation and use of *nonlinear stability estimates* based on the notion of entropy function [41, 42]. The approach resembles closely the classical energy method for incompressible Navier–Stokes equations [43, 44], where the control of total kinetic energy has been in the very heart of the existence proofs. Many existing discrete schemes, starting from early FD approximations and recent FE models [45], are built upon this principle, yielding stable and accurate approximations. This is precisely the idea motivating the present work.

Outline of the Work

We start with a short review of the governing equations and the notation of the abstract entropy function. A number of specific problems of interest are briefly discussed. In Section 3 we derive and discuss the fundamental nonlinear stability estimate. Section 4 is devoted to a discussion on the possibility of constructing FE schemes which would satisfy the same stability result at the discrete level. As a conclusion, two numerical strategies, one for transient and one for steady-state simulations, are proposed and illustrated with a number of numerical examples (Section 5).

2. COMPRESSIBLE NAVIER–STOKES EQUATIONS AND THE ENTROPY FUNCTION

We shall study a general class of compressible flow equations of the form

$$\mathbf{U}_{,t} + \mathbf{f}^i(\mathbf{U})_{,i} = (\mathbf{K}^{ij}\mathbf{U}_{,j})_{,i}, \tag{2.1}$$

where

- $U \in \mathbb{R}^m$, $\mathbf{U} = \mathbf{U}(t, \mathbf{x})$ denotes the vector of unknown state functions of time t and space variable $\mathbf{x} \in \mathbb{R}^n$, $n =$ 2 or 3,
- $\mathbf{f}^i = \mathbf{f}^i(\mathbf{U})$ are given algebraic functions defined in some open set of $\mathbb{R}^m$ with values in $\mathbb{R}^m$,
- $\mathbf{K}^{ij} = \mathbf{K}^{ij}(\mathbf{U}, \mathbf{U}_{,1}, ..., \mathbf{U}_{,n})$ are given functions of state variable $\mathbf{U} \in \mathbb{R}^m$ and its spatial gradient components.

Commas, as usual, denote the differentiation with respect to time or spatial variables, respectively.

An algebraic, scalar-valued function $H = H(\mathbf{U})$ is called an *entropy function* for system (2.1) if it satisfies the following three conditions:

1. H is a strictly convex function of $\mathbf{U}$,
2. there exist functions $F^i = F^i(\mathbf{U})$, $i = 1, ..., n$, called the *entropy fluxes*, such that

$$H_{,\mathbf{U}}\mathbf{f}^i_{,\mathbf{U}} = F^i_{,\mathbf{U}}, \tag{2.2}$$

and

3.

$$\mathbf{U}_i^{\mathrm{T}} H_{,\mathbf{UU}} \mathbf{K}^{ij}(\mathbf{U}, \mathbf{U}_1, ..., \mathbf{U}_n)\mathbf{U}_i \geq 0 \quad \forall(\mathbf{U}_1, ..., \mathbf{U}_n). \quad (2.3)$$

In particular, the second condition implies the symmetrizing property of Hessian $H_{,\mathbf{UU}} =: \mathbf{A}_0$, called frequently the *symmetrizer*

$$(\mathbf{A}_0\mathbf{A}^i)^{\mathrm{T}} = \mathbf{A}_0\mathbf{A}^i, \quad i = 1, ..., n, \quad (2.4)$$

where $\mathbf{A}^i = \mathbf{f}^i_{,\mathbf{U}}$ are the Jacobian matrices.

The following problems fall into the prescribed category.

Compressible Navier–Stokes Equations

The vector of unknowns $\mathbf{U} = (\rho, \rho u_1, ..., \rho u_n, e)^{\mathrm{T}}$ includes density ρ, momentum components ρu_i, where u_i- are the velocity components, and total energy density e. Functions $\mathbf{f}^i(\mathbf{U})$ and $\mathbf{K}^{ij} = \mathbf{K}^{ij}(\mathbf{U})$ are the usual Eulerian fluxes and viscous matrices, respectively. The entropy function is identified as the (negative) actual entropy density function $H = \rho \ln(p\rho^{-\gamma})$ (where p and γ denote the pressure and the ratio of specific heats) with the corresponding fluxes equal to the actual entropy fluxes $F^i = Hu_i$. For algebraic details, see [41, 46].

Compressible Euler Equations

This is simply a simplified version of the Navier–Stokes equations with all viscous matrices set to zero.

Regularized Euler Equations

In this case matrices $\mathbf{K}^{ij}$ correspond to various regularizations of the Euler equations performed explicitly or resulting implicitly from various time discretization schemes. Two particular cases of interest include matrices $\mathbf{K}^{ij}_T$ resulting from the Taylor–Galerkin method discussed in subsequent sections

$$\mathbf{K}^{ij}_T = \frac{\Delta t}{2}\mathbf{f}^i_{,\mathbf{U}}\mathbf{f}^j_{,\mathbf{U}} = \frac{\Delta t}{2}\mathbf{A}^i\mathbf{A}^j \quad (2.5)$$

and the artificial viscosity term proposed by Johnson *et al.* [47, 28] and Hughes *et al.* [18],

$$\mathbf{K}^{ij}_N = Ch\frac{\mathbf{f}^k_{,k}\mathbf{H}_{,\mathbf{UU}}\mathbf{f}^k_{,k}}{\mathbf{U}_{,l}H_{,\mathbf{UU}}\mathbf{U}_{,l}}\delta_{ij}\mathbf{I} = Ch\alpha_N\delta_{ij}\mathbf{I} \quad (2.6)$$

where C is a positive parameter, Δt is a time step, and h is an element size.

In both cases condition (2.3) is satisfied. Indeed, for the Taylor–Galerkin terms we have

$$\begin{aligned}\mathbf{U}_i^{\mathrm{T}} H_{,\mathbf{UU}}\mathbf{K}^{ij}_T\mathbf{U}_j &= \frac{\Delta t}{2}\mathbf{U}_i^{\mathrm{T}}\mathbf{A}_0\mathbf{A}^i\mathbf{A}^j\mathbf{U}_j \\ &= \frac{\Delta t}{2}\mathbf{U}_i^{\mathrm{T}}(\mathbf{A}_0\mathbf{A}^i)^{\mathrm{T}}\mathbf{A}^j\mathbf{U}_j \\ &= \frac{\Delta t}{2}\mathbf{U}_i^{\mathrm{T}}(\mathbf{A}^i)^{\mathrm{T}}\mathbf{A}_0\mathbf{A}^j\mathbf{U}_j \\ &= \frac{\Delta t}{2}(\mathbf{A}^i\mathbf{U}_i)^{\mathrm{T}}\mathbf{A}_0(\mathbf{A}^j\mathbf{U}_j) \geq 0\end{aligned} \quad (2.7)$$

and

$$\begin{aligned}\mathbf{U}_i^{\mathrm{T}} H_{,\mathbf{UU}}\mathbf{K}^{ij}_N\mathbf{U}_j &= \mathbf{U}_i^{\mathrm{T}} H_{,\mathbf{UU}} Ch\frac{\mathbf{f}^k_{,k}H_{,\mathbf{UU}}\mathbf{f}^k_{,k}}{\mathbf{U}_{,l}H_{,\mathbf{UU}}\mathbf{U}_{,l}}\delta_{ij}\mathbf{I}\mathbf{U}_j \\ &= Ch\frac{\mathbf{f}^k_{,k}H_{,\mathbf{UU}}\mathbf{f}^k_{,k}}{\mathbf{U}_{,l}H_{,\mathbf{UU}}\mathbf{U}_{,l}}\mathbf{U}_i^{\mathrm{T}} H_{,\mathbf{UU}}\mathbf{U}_i \\ &\geq 0.\end{aligned} \quad (2.8)$$

In (2.7) and (2.8) we used the symmetry of $\mathbf{A}_0\mathbf{A}^i$ and the positive definitness of $\mathbf{A}_0$.

Isentropic Flow

In this simplified version of the compressible flow equations, the entropy is assumed constant throughout the domain, the energy balance equation is neglected, and the remaining mass and momentum equations are solved for density and momentum components $\mathbf{U} = (\rho, \rho u_1, ..., \rho u_n)^{\mathrm{T}}$. The abstract entropy function is now identified as the total energy,

$$H = e = \rho\frac{u_i u_i}{2} + \frac{1}{\gamma - 1}A\rho^{\gamma}, \quad (2.9)$$

where $p = A\rho^{\gamma}$, $A = A(s)$ const (see [48]), and the entropy fluxes are given by

$$F^i = (\rho e + p)u_i. \quad (2.10)$$

We conclude this section with the notion of the modified entropy function (see [49, 41]). Given a particular system of Eqs. (2.1) and a corresponding entropy function $H = H(\mathbf{U})$, we select an arbitrary *constant* $\overline{\mathbf{U}}$ from the domain of definition of function H and define the *modified entropy function*

$$\hat{H}(\mathbf{U}) = H(\mathbf{U}) - H(\overline{\mathbf{U}}) - H_{,\mathbf{U}}(\overline{\mathbf{U}})(\mathbf{U} - \overline{\mathbf{U}}) \quad (2.11)$$

and the corresponding *modified entropy fluxes*

$$\hat{F}^i(\mathbf{U}) = F^i(\mathbf{U}) - H_{,\mathbf{U}}(\overline{\mathbf{U}})(\mathbf{f}^i(\mathbf{U}) - \mathbf{f}^i(\overline{\mathbf{U}})). \quad (2.12)$$

It can be verified that the modified entropy function and

the corresponding modified entropy fluxes satisfy conditions (2.1)–(2.3). In other words, once a particular entropy function exists, we have automatically a whole, one-parameter $\overline{\mathbf{U}}$, family of them. The essential difference between the original and the modified entropy functions is that, contrary to $H(\mathbf{U})$, the modified function $\hat{H}(\mathbf{U})$ is always positive semidefinite and it may serve as a *norm-like* quantity to measure distance between two different solutions to the problem.

Finally, we record explicit formulas for the modified entropy function and its corresponding modified entropy fluxes for the Euler equations

$$\begin{aligned}
\hat{H}(\mathbf{U}) &= \hat{H}(\rho, u_1, ..., u_n, p) \\
&= -\rho\left(\frac{H}{\rho} - \frac{\overline{H}}{\overline{\rho}}\right) - \gamma(\rho - \overline{\rho}) + \frac{\overline{\rho}}{\overline{p}}(p - \overline{p}) \\
&\quad + (\gamma - 1)\frac{\overline{\rho}}{\overline{p}}\rho\frac{1}{2}\sum_{i=1}^{n}(u_i - \overline{u}_i)^2 \\
\hat{F}^i(\mathbf{U}) &= \hat{F}^i(\rho, u_1, ..., u_n, p) \\
&= \hat{H}u_i + (\gamma - 1)\frac{\overline{\rho}}{\overline{p}}(u_i - \overline{u}_i)(p - \overline{p}) \\
&= -\rho u_i\left[\ln\left(\frac{p}{\rho^\gamma}\frac{\overline{\rho}^\gamma}{\overline{p}}\right) - \underline{\gamma\frac{p}{\rho}\frac{\overline{\rho}}{\overline{p}}} + \gamma\right] \\
&\quad + (\gamma - 1)\frac{\overline{\rho}}{\overline{p}}\left[u_i\rho\frac{1}{2}\sum_i(u_i - \overline{u}_i)^2 - \overline{u}_i(p - \overline{p})\right],
\end{aligned} \tag{2.13}$$

where $\overline{\rho}, \overline{u}_1, ..., \overline{u}_n, \overline{p}$ correspond to the reference vector $\overline{\mathbf{U}}$. The underlined term is apparently missing in the formula provided in [41].

3. NONLINEAR STABILITY

Let $\mathbf{U} = \mathbf{U}(\mathbf{x}, t)$ be a solution to Eqs. (2.1) and $\overline{\mathbf{U}}$ a selected *reference vector*. Multiplying Eqs. (2.1) by $\hat{H}_{,\mathbf{U}}$, where $\hat{H}$ is the modified entropy function, we get

$$\hat{H}_{,\mathbf{U}} + \hat{H}_{,\mathbf{U}}\mathbf{f}^i_{,\mathbf{U}}\mathbf{U}_{,i} = \hat{H}_{,\mathbf{U}}(\mathbf{K}^{ij}\mathbf{U}_{,j})_{,i}, \tag{3.1}$$

or, equivalently,

$$\begin{aligned}
\hat{H}_{,t} + \hat{F}^i_{,t} &= (\hat{H}_{,\mathbf{U}}\mathbf{K}^{ij}\mathbf{U}_{,\mathrm{j}})_{,i} - (\hat{H}_{,\mathbf{U}})_{,t}\mathbf{K}^{ij}\mathbf{U}_{,j} \\
&= (\hat{H}_{,\mathbf{U}}\mathbf{K}^{ij}\mathbf{U}_{,\mathrm{j}})_{,i} - \mathbf{U}_{,i}H_{,\mathbf{UU}}\mathbf{K}^{ij}\mathbf{U}_{,j}.
\end{aligned} \tag{3.2}$$

Integrating over a computational domain $\Omega \subset \mathbb{R}^n$ and using the divergence theorem, we get

$$\begin{aligned}
&\frac{d}{dt}\int_\Omega \hat{H}\,d\mathbf{x} + \int_\Gamma(\hat{F}^i - \hat{H}_{,\mathbf{U}}\mathbf{K}^{ij}\mathbf{U}_{,j})n_i\,ds \\
&= -\int_\Omega \mathbf{U}_{,i}H_{,\mathbf{UU}}\mathbf{K}^{ij}\mathbf{U}_{,j}\,d\mathbf{x} \le 0,
\end{aligned} \tag{3.3}$$

where Γ is the boundary of domain Ω and n_i denote components of the outward unit normal vector.

Integrating in time over a $(0, t)$ interval, we obtain another, equivalent form of the same result,

$$\begin{aligned}
\left(\int_\Omega \hat{H}\,d\mathbf{x}\right)(t) &\le \left(\int_\Omega \hat{H}\,d\mathbf{x}\right)(0) \\
&\quad + \int_0^t\int_\Gamma(\hat{F}^i - \hat{H}_{,\mathbf{U}}\mathbf{K}^{ij}\mathbf{U}_{,j})n_i\,ds\,dt.
\end{aligned} \tag{3.4}$$

We refer to (3.3) or (3.4) as the *nonlinear stability* result.

Connection with a Linear Stability Analysis

For solutions $\mathbf{U}$ close to the reference vector $\overline{\mathbf{U}}$, i.e., for small perturbations $\boldsymbol{\delta}\mathbf{U} = \mathbf{U} - \overline{\mathbf{U}}$, the modified entropy function reduces to a quadratic energy-like functional of $\boldsymbol{\delta}\mathbf{U}$,

$$\hat{H}(\mathbf{U}) \approx \tfrac{1}{2}\,\boldsymbol{\delta}\mathbf{U}^{\mathrm{T}}H_{,\mathbf{UU}}(\overline{\mathbf{U}})\boldsymbol{\delta}\mathbf{U} \tag{3.5}$$

and the whole stability result reduces to the classical energy method applied to the linearized and localized problem

$$\boldsymbol{\delta}\mathbf{U}_{,t} + \mathbf{A}^i(\overline{\mathbf{U}})\boldsymbol{\delta}\mathbf{U}_{,i} = (\mathbf{K}^{ij}(\overline{\mathbf{U}})\boldsymbol{\delta}\mathbf{U}_{,j})_{,i}. \tag{3.6}$$

Accordingly, the final linear stability result is in the form

$$\begin{aligned}
&\frac{1}{2}\frac{d}{dt}\int_\Omega \boldsymbol{\delta}\mathbf{U}^{\mathrm{T}}\mathbf{A}_0\boldsymbol{\delta}\mathbf{U}\,d\mathbf{x} + \int_\Gamma(\boldsymbol{\delta}\mathbf{U}^{\mathrm{T}}\mathbf{A}_0\mathbf{A}^i n_i\boldsymbol{\delta}\mathbf{U} \\
&\quad - \boldsymbol{\delta}\mathbf{U}^{\mathrm{T}}\mathbf{A}_0\mathbf{K}^{ij}n_i\boldsymbol{\delta}\mathbf{U}_{,j})\,ds \\
&= -\int_\Omega \boldsymbol{\delta}\mathbf{U}_{,i}\mathbf{A}_0\mathbf{K}^{ij}\boldsymbol{\delta}\mathbf{U}_{,j}\,d\mathbf{x} \le 0,
\end{aligned} \tag{3.7}$$

where symmetrizer $\mathbf{A}_0 = H_{,\mathbf{UU}}$, Jacobian matrices $\mathbf{A}^i = \mathbf{f}^i_{,\mathbf{U}}$ and viscous matrices $\mathbf{K}^{ij}$, are all evaluated at $\overline{\mathbf{U}}$.

Stability estimate (3.7) may serve as a basis for designing stable open boundary conditions for system (3.6) and, in particular, for determining the right number of supersonic/subsonic inflow/outflow boundary conditions for Euler equations (see [37, 40, 50]).

Entropy Controlled Simulations

One conclusion which can certainly be drawn from inequality (3.3) is that, for any solution $\mathbf{U}$ of system (2.1) and arbitrary domain Ω, independently of boundary conditions, there must be

$$\frac{d}{dt}\int_\Omega \hat{H}\,d\mathbf{x} + \int_\Gamma(\hat{F}^i - \hat{H}_{,\mathbf{U}}\mathbf{K}^{ij}\mathbf{U}_{,j})n_i\,ds \le 0. \tag{3.8}$$

As the right-hand side in (3.3) is independent of reference

vector $\overline{\mathbf{U}}$, this stability estimate is equivalent to the global (original) entropy dissipation inequality of the same form

$$\frac{d}{dt}\int_\Omega H\,d\mathbf{x} + \int_\Gamma (F^i - H_{,\mathbf{U}}\mathbf{K}^{ij}\mathbf{U}_{,j})n_i\,ds \le 0. \quad (3.9)$$

It is exactly the inequality we will try to enforce on the discrete level in our finite element simulations described in the next section.

4. FINITE ELEMENT APPROXIMATIONS; DISCRETE STABILITY

For the sake of precision, we begin by formally restating the initial-boundary value problem of interest.

Given a computational domain $\Omega \subset \mathbb{R}^2$ we wish to determine the solution $\mathbf{U} = \mathbf{U}(\mathbf{x}, t)$, $\mathbf{x} \in \Omega$, $t > 0$, $\mathbf{U} = (\rho, m_1, m_2, e)^{\mathrm{T}}$, satisfying

- the regularized Euler equations,

$$\mathbf{U}_{,t} + \mathbf{f}^i(\mathbf{U})_{,i} = (\mathbf{K}^{ij}(\mathbf{U}, \nabla\mathbf{U})\mathbf{U}_{,j})_{,i}, \quad (4.1)$$

where $\mathbf{f}^i(\mathbf{U})$ are the Eulerian fluxes, and $\mathbf{K}^{ij} = \mathbf{K}^{ij}(\mathbf{U}, \nabla\mathbf{U})$ are some particular (to be specified later) regularizing terms,

- inflow boundary conditions,

$$\mathbf{U}(\mathbf{x}, t) = \mathbf{U}^\infty \quad \text{on } \Gamma^{\text{in}} \quad (4.2)$$

- outflow boundary conditions,

$$\mathbf{U}_{,n} = \mathbf{0} \quad \text{on } \Gamma^{\text{out}} \quad (4.3)$$

- solid wall boundary conditions,

$$u_n = 0, \quad \rho_{,n} = e_{,n} = u_{t,n} = 0 \quad \text{on } \Gamma^w, \quad (4.4)$$

where u_n and u_t denote the normal and tangential components of the velocity vector,

- initial condition,

$$\mathbf{U}(\mathbf{x}, 0) = \mathbf{U}^0(\mathbf{x}). \quad (4.5)$$

In all the subsequently considered examples, the classification of the boundary into inflow, outflow, and solid wall (symmetry) parts of the boundary is fixed and it is not subjected to a change during the simulations. Initial condition function $\mathbf{U}^0(\mathbf{x})$ is compatible with the boundary conditions. Note that, in particular, we do not distinguish between supersonic/subsonic inflow or outflow boundaries.

Method of Discretization in Time

We solve the problem by using a finite-difference approximation in time, combined with the finite-element approximation in space variables. Keeping in mind adaptivity in space variables, resulting in a time-varying space approximation, we employ the so-called *method of discretization in time,* known also as the *Rothe method,* rather than the standard method of lines. The final formulation is obtained in two steps. Given a sequence of time instants

$$0 = t_0 < t_1 < \cdots < t_n, \quad (4.6)$$

where $t_n = n\,\Delta t$ and Δt = some constant time step; we first replace the original equation with a sequence of steady-state like problems to be solved for $\mathbf{U}^n(\mathbf{x}) \approx \mathbf{U}(\mathbf{x}, t_n)$. In the second step we consider a typical one-step problem and develop a corresponding variational formulation, laying down a foundation for standard, continuous FE discretizations.

Time Discretization Schemes

Two time discretization schemes are considered:

- first-order implicit Euler scheme,

$$\mathbf{U}(t + \Delta t) - \Delta t\mathbf{U}_{,t}(t + \Delta t) = \mathbf{U}(t) + O(\Delta t^2), \quad (4.7)$$

- second-order Lax–Wendroff time-stepping scheme,

$$\mathbf{U}(t + \Delta t) - \frac{\Delta t^2}{2}\mathbf{U}_{,tt}(t + \Delta t) = \mathbf{U}(t) + \Delta t\mathbf{U}_{,t}(t) + O(\Delta t^3). \quad (4.8)$$

Using (4.1) we represent the time derivatives in terms of spatial derivatives:

$$\begin{aligned}
\mathbf{U}_{,t} &= (\mathbf{K}^{ij}\mathbf{U}_{,j})_{,i} - \mathbf{f}^i(\mathbf{U})_{,i} \\
\mathbf{U}_{,tt} &= (\mathbf{K}^{ij}\mathbf{U}_{,j})_{,it} - \mathbf{f}^i(\mathbf{U})_{,it} \\
&= (\mathbf{K}^{ij}\mathbf{U}_{,j})_{,it} - (\mathbf{A}^i(\mathbf{U})\mathbf{U}_{,t})_{,i} \\
&= (\mathbf{K}^{ij}\mathbf{U}_{,j})_{,it} + (\mathbf{A}^i(\mathbf{U})\mathbf{A}^j(\mathbf{U})\mathbf{U}_{,j})_{,i} - (\mathbf{A}^i(\mathbf{U})(\mathbf{K}^{jl}\mathbf{U}_{,l})_{,j})_{,i}.
\end{aligned} \quad (4.9)$$

Finally, assuming that the artificial viscosity term and its derivatives are of order Δt away from shocks, we substitute (4.9) into (4.7) and (4.8), we neglect the terms of order higher than one for (4.7), and higher than two for (4.8), and arrive at the two following schemes:

- *nonlinear*, first-order, implicit Euler scheme,

$$\mathbf{U}^{n+1} + \Delta t\mathbf{f}^i(\mathbf{U}^{n+1})_{,i} - \Delta t(\mathbf{K}^{ij}(\mathbf{U}^{n+1})\mathbf{U}^{n+1}_{,j})_{,i} = \mathbf{U}^n, \quad (4.10)$$

- *linear*, second-order, implicit Lax–Wendroff scheme,

$$\mathbf{U}^{n+1} - \frac{\Delta t^2}{2}(\mathbf{A}^i(\mathbf{U}^n)\mathbf{A}^j(\mathbf{U}^n)\mathbf{U}^{n+1}_{,j})_{,i} - \Delta t(\mathbf{K}^{ij}(\mathbf{U}^n)\mathbf{U}^{n+1}_{,j})_{,i} = \mathbf{U}^n - \Delta t\mathbf{f}^i(\mathbf{U}^n)_{,i}. \tag{4.11}$$

Finally we notice that Eq. (4.11) can be viewed as a first sweep of iterations for solving the implicit Euler step with viscous matrices defined as the sum of viscous matrices used in (4.10) and the extra second-order term resulting from the second-order approximation in time,

$$_{\text{new}}\mathbf{K}^{ij} = {}_{\text{old}}\mathbf{K}^{ij} + \frac{\Delta t}{2}\mathbf{A}^i\mathbf{A}^j. \tag{4.12}$$

More precisely, introducing the iterates

$$\mathbf{U}^n = \mathbf{U}^{n,0}, \mathbf{U}^{n,1}, ..., \mathbf{U}^{n,k-1}, \mathbf{U}^{n,k}, ..., \mathbf{U}^{n+1}, \tag{4.13}$$

we calculate the intermediate solution $\mathbf{U}^{n,k}$ by solving

$$\mathbf{U}^{n+1,k} - \frac{\Delta t^2}{2}(\mathbf{A}^i(\mathbf{U}^{n,k-1})\mathbf{A}^j(\mathbf{U}^{n,k-1})\mathbf{U}^{n,k}_{,j})_{,i} - \Delta t(\mathbf{K}^{ij}(\mathbf{U}^{n,k-1})\mathbf{U}^{n,k}_{,j})_{,i} = \mathbf{U}^n - \Delta t(\mathbf{f}^i(\mathbf{U}^{n,k-1}))_{,i}. \tag{4.14}$$

Finally, we specify the artificial viscosity terms $\mathbf{K}^{ij} = \mathbf{K}^{ij}_N$, with $\mathbf{K}^{ij}_N$ given by (2.6), where $C = C(t)$ is a time-varying constant, $h = h(\mathbf{x}, t)$ is a mesh density function, and $\mathbf{K}^{ij} = \mathbf{K}^{ij}_N + \Delta t/2\mathbf{A}^i\mathbf{A}^j$ for the Euler scheme. According to the remark just made, this corresponds to using the Lax–Wendroff scheme to converge to a steady state solution.

Nonlinear Time Stability Analysis

Multiplying (4.10) by $H_{,\mathbf{U}}(\mathbf{U}^{n+1})$, integrating over computational domain Ω, and neglecting the boundary terms corresponding to matrices $\mathbf{K}^{ij}$ (or, equivalently, assuming appropriate homogeneous boundary conditions), we get

$$\int_\Omega H^{n+1}_{,\mathbf{U}}(\mathbf{U}^{n+1} - \mathbf{U}^n) + \Delta t\int_\Omega H^{n+1}_{,\mathbf{U}}\mathbf{f}^i(\mathbf{U}^{n+1})_{,i} = -\Delta t\int_\Omega (\mathbf{U}^{n+1}_{,i})^{\mathrm{T}}H^{n+1}_{,\mathbf{UU}}\mathbf{K}^{ij}(\mathbf{U}^{n+1})\mathbf{U}^{n+1}_{,j} \le 0, \tag{4.15}$$

where $H^{n+1}_{,\mathbf{U}} = H_{,\mathbf{U}}(\mathbf{U}^{n+1})$ and $H^{n+1}_{,\mathbf{UU}} = H_{,\mathbf{UU}}(\mathbf{U}^{n+1})$.

Due to the convexity of entropy function H, the first term on the left-hand side of (4.15) can be bounded below by

$$H^{n+1}_{,\mathbf{U}}(\mathbf{U}^{n+1} - \mathbf{U}^n) \ge H_{,\mathbf{U}|\mathbf{U}^n+\tau(\mathbf{U}^{n+1}-\mathbf{U}^n)}(\mathbf{U}^{n+1} - \mathbf{U}^n) = (d/d\tau)H(\mathbf{U}^n + \tau(\mathbf{U}^{n+1} - \mathbf{U}^n)). \tag{4.16}$$

Integrating (4.16) with respect to τ from 0 to 1, we get

$$H^{n+1}_{,\mathbf{U}}(\mathbf{U}^{n+1} - \mathbf{U}^n) \ge H(\mathbf{U}^{n+1}) - H(\mathbf{U}^n). \tag{4.17}$$

Combining (4.17) with (4.15) we get the final result,

$$\int_\Omega H(\mathbf{U}^{n+1}) - \int_\Omega H(\mathbf{U}_n) + \Delta t\int_\Gamma F^i(\mathbf{U}^{n+1})n_i \le -\Delta t\int_\Omega (\mathbf{U}^{n+1}_{,i})^{\mathrm{T}}H^{n+1}_{,\mathbf{UU}}\mathbf{K}^{ij}(\mathbf{U}^{n+1})\mathbf{U}^{n+1}_{,j}, \le 0, \tag{4.18}$$

which can be viewed as a discrete counterpart of the continuous stability inequality (3.3). We emphasize that the entropy function can be replaced with the modified entropy function, with any reference vector $\overline{\mathbf{U}}$. Thus the *Euler implicit scheme is unconditionally stable* from the point of view of this nonlinear estimate.

An analogous result for the second-order scheme does not hold. Denoting by $\mathbf{K}^{ij}$ the sum of the original regularizing terms and the second-order term, we can rewrite it in the form

$$\mathbf{U}^{n+1} - \mathbf{U}^n + \Delta t\mathbf{f}^i(\mathbf{U}^n)_{,i} - \Delta t(\mathbf{K}^{ij}(\mathbf{U}^n)\mathbf{U}^{n+1}_{,j})_{,i} = \mathbf{0} \tag{4.19}$$

and, after performing an analysis similar to that for the first-order scheme, we get

$$\int_\Omega H(\mathbf{U}^{n+1}) - \int_\Omega H(\mathbf{U}^n) + \Delta t\int_\Gamma F^i(\mathbf{U}^{n+1})n_i \le -\Delta t\int_\Omega (\mathbf{U}^{n+1}_{,t})^{\mathrm{T}}H^{n+1}_{,\mathbf{UU}}\mathbf{K}^{ij}(\mathbf{U}^n)\mathbf{U}^{n+1}_{,j} + \Delta t\int_\Omega (H_{,\mathbf{U}}(\mathbf{U}^{n+1}) - H_{,\mathbf{U}}(\mathbf{U}^n))\mathbf{f}^i(\mathbf{U}^n)_{,i}. \tag{4.20}$$

To make the right-hand side of (4.20) negative, the following two remedies are possible. One is to decrease the time step, so that the next step solution $\mathbf{U}^{n+1}$ would get closer to $\mathbf{U}^n$. Another one is to increase the dissipation by increasing the constant C in (2.6). We shall discuss the second option in the end of this section.

Variational Formulation of the One-Step Problem

We follow the standard procedure to derive the variational formulation of the one-step problems (4.11) and (4.14). First we introduce the set of kinematically admissible functions $\mathbf{X}$ consisting of all functions $\mathbf{U}$ satisfying the nonhomogeneous Dirichlet boundary conditions (4.2) and $(4.4)_1$. Next we define the corresponding space $\mathbf{V}$ consisting of functions satisfying the homogeneous version of the same conditions. Finally, we multiply (4.11) by a test function $\mathbf{W}$ and integrate over domain Ω to obtain

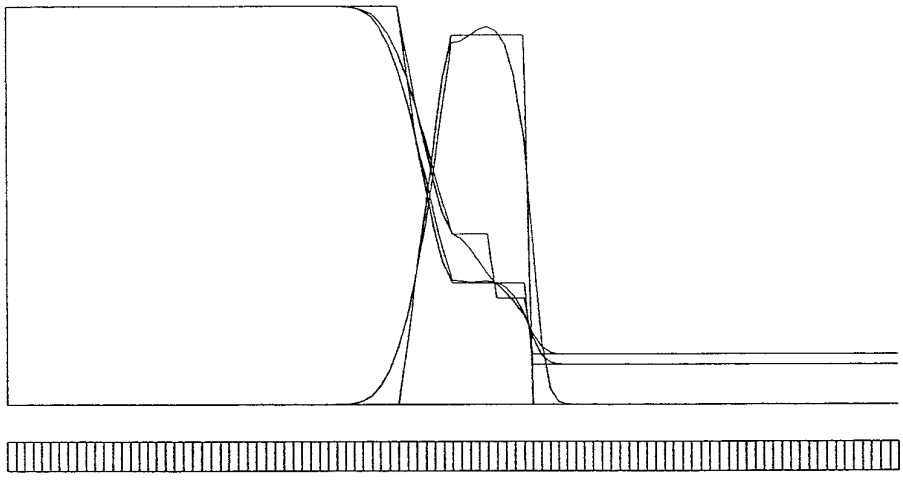

FIG. 1. Shock tube problem: density, velocity, and pressure after 0.05s ($C_0 = 0.3$).

$$\int_\Omega \mathbf{W}^{\mathrm{T}}\mathbf{U}^{n+1} - \frac{\Delta t^2}{2}\int_\Omega \mathbf{W}^{\mathrm{T}}(\mathbf{A}^i(\mathbf{U}^n)\mathbf{A}^j(\mathbf{U}^n)\mathbf{U}^{n+1}_{,j})_{,i} - \Delta t\int_\Omega \mathbf{W}^{\mathrm{T}}(\mathbf{K}^{ij}_N(\mathbf{U}^n)\mathbf{U}^{n+1}_{,j})_{,i} = \int_\Omega \mathbf{W}^{\mathrm{T}}\mathbf{U}^n - \Delta t\int_\Omega \mathbf{W}^{\mathrm{T}}\mathbf{f}^i(\mathbf{U}^n)_{,i}. \tag{4.21}$$

Integration by parts yields

$$\frac{\Delta t^2}{2}\int_\Omega \mathbf{W}^{\mathrm{T}}(\mathbf{A}^i(\mathbf{U}^n)\mathbf{A}^j(\mathbf{U}^n)\mathbf{U}^{n+1}_{,j})_{,i}\,d\mathbf{x} = \frac{\Delta t^2}{2}\int_\Omega \mathbf{W}^{\mathrm{T}}_{,i}\mathbf{A}^i(\mathbf{U}^n)\mathbf{A}^j(\mathbf{U}^n)\mathbf{U}^{n+1}_{,j}\,d\mathbf{x} - \frac{\Delta t^2}{2}\int_\Gamma \mathbf{W}^{\mathrm{T}}\mathbf{A}^i(\mathbf{U}^n)\mathbf{A}^j(\mathbf{U}^n)\mathbf{U}^{n+1}_{,j}n_j\,ds \tag{4.22}$$

and

$$-\Delta t\int_\Omega \mathbf{W}^{\mathrm{T}}(\mathbf{K}^{ij}_N(\mathbf{U}^n)\mathbf{U}^{n+1}_{,j})_{,i}\,d\mathbf{x} = \Delta t\int_\Omega \mathbf{W}^{\mathrm{T}}_{,i}\mathbf{K}^{ij}_N(\mathbf{U}^n)\mathbf{U}^{n+1}_{,j}\,d\mathbf{x} - \Delta t\int_\Gamma \mathbf{W}^{\mathrm{T}}\mathbf{K}^{ij}_N(\mathbf{U}^n)\mathbf{U}^{n+1}_{,j}n_i\,ds. \tag{4.23}$$

It follows from formula (2.6) and the boundary conditions that the boundary term in (4.23) vanishes. Some boundary terms in (4.22) are left, but they are neglected in computations, which is formally equivalent to a modification of the natural boundary conditions by the second-order (in time) terms.

Finally, integrating by parts also the right-hand side of (4.21) we arrive at the variational formulation in the form

Find $\mathbf{U}^{n+1} \in \mathbf{X}$ such that

$$\int_\Omega \mathbf{W}^{\mathrm{T}}\mathbf{U}^{n+1}\,d\mathbf{x} + \int_\Omega \mathbf{W}^{\mathrm{T}}_{,i}\left(\Delta t\,\mathbf{K}^{ij}_N(\mathbf{U}^n) + \frac{\Delta t^2}{2}\mathbf{A}^i(\mathbf{U}^n)\mathbf{A}^j(\mathbf{U}^n)\right)\mathbf{U}^{n+1}_{,j}\,d\mathbf{x} = \int_\Omega \mathbf{W}^{\mathrm{T}}\mathbf{U}^n\,d\mathbf{x} + \Delta t\int_\Omega \mathbf{W}^{\mathrm{T}}_{,i}\mathbf{f}^i(\mathbf{U}^n)\,d\mathbf{x} - \Delta t\int_\Gamma \mathbf{W}^{\mathrm{T}}\mathbf{f}^i(\mathbf{U}^n)n_i\,ds \tag{4.24}$$

for every $\mathbf{W} \in \mathbf{V}$.

In the same way we derive the variational formulation for (4.14).

The final, one-step discretized problem is obtained by replacing $\mathbf{X}$ and $\mathbf{V}$ with some finite-dimensional subspaces $\mathbf{X}_h$ of $\mathbf{X}$ and $\mathbf{V}_h$ of $\mathbf{V}$, resulting from a particular FE mesh. We mention that the bilinear form defining the left-hand side satisfies the LBB (Ladyzhenskaya–Babuška–Brezzi) condition (see [51] for details) and that the scheme is conservative which can be seen by substituting for $\mathbf{W}$ in (4.24) a constant.

Linear Stability Analysis

The result of solving the discrete counterpart of (4.24) can be written as

$$\mathbf{U}^{n+1}_h = T\mathbf{U}^n_h, \tag{4.25}$$

where T is the finite element operator implicitly defined by (4.24). To investigate the stability properties of T we limit ourselves to a system of linear equations with constant coefficients. This corresponds to considering linear system

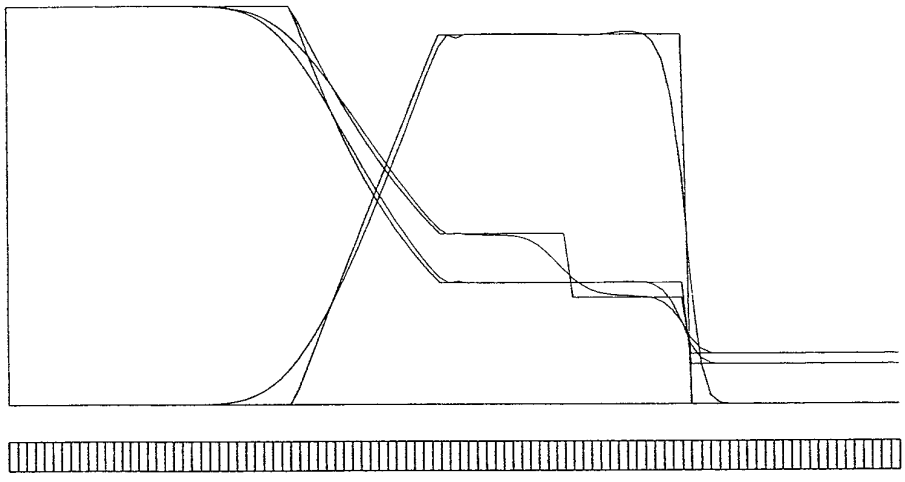

FIG. 2. Shock tube problem: density, velocity, and pressure after 0.15s ($C_0 = 0.3$).

(3.20) resulting from the linearization of the equations around some *constant* state $\overline{\mathbf{U}}$. Furthermore, due to the presence of first-order terms, the operator T is not self-adjoint and to analyze it we have to consider its complex extension [23]. To this end, we assume that $\mathbf{W}$, $\mathbf{U}_h^n$, and $\mathbf{U}_h^{n+1}$ are complex and exchange $\mathbf{W}_h^{\mathrm{T}}$ for its complex conjugate $\overline{\mathbf{W}}_h^{\mathrm{T}}$.

We investigate the stability properties of T by estimating its *complex* eigenvalues. Let us assume that $\mathbf{U}_h^n$ is an eigenvector and substitute into (4.24) $\mathbf{U}_h^{n+1} = \lambda \mathbf{U}_h^n$, with λ the corresponding eigenvalue. Selecting $\mathbf{W}_h = \overline{H}_{,\mathbf{UU}} = H_{,\mathbf{UU}}(\overline{\mathbf{U}})\mathbf{U}_h^n$, we obtain

$$\begin{aligned}
&\lambda \int_\Omega (\overline{\mathbf{U}}_h^n)^{\mathrm{T}} \overline{H}_{,\mathbf{UU}} \mathbf{U}_n^h \, d\mathbf{x} \\
&\quad + \lambda \, \Delta t \int_\Gamma \frac{\Delta t}{2} (\overline{\mathbf{U}}_h^n)_{,i}^{\mathrm{T}} \overline{A}^i \overline{H}_{,\mathbf{UU}} \overline{A}^j (\mathbf{U}_h^n)_{,j} \, d\mathbf{x} \\
&\quad + \lambda C \, \Delta t \int_\Omega h (\overline{\mathbf{U}}_h^n)_{,i}^{\mathrm{T}} \overline{H}_{,\mathbf{UU}} (\mathbf{U}_h^n)_{,i} \\
&\qquad \frac{(\overline{\mathbf{U}}_h^n)^{\mathrm{T}} \overline{\mathbf{A}}^i \overline{H}_{,\mathbf{UU}} \overline{\mathbf{A}}^j (\mathbf{U}_h^n)_{,j}}{(\overline{\mathbf{U}}_h^n)_{,j}^{\mathrm{T}} \overline{H}_{,\mathbf{UU}} (\mathbf{U}_h^n)_{,j}} \, d\mathbf{x} \\
&= \int_\Omega (\overline{\mathbf{U}}_h^n)^{\mathrm{T}} \overline{H}_{,\mathbf{UU}} \mathbf{U}_h^n \, d\mathbf{x} + \Delta t \int_\Omega (\overline{\mathbf{U}}_h^n)_{,i}^{\mathrm{T}} \overline{H}_{,\mathbf{UU}} \overline{\mathbf{A}}^j \mathbf{U}_h^n \, d\mathbf{x} \\
&\quad - \Delta t \int_\Gamma (\overline{\mathbf{U}}_h^n)^{\mathrm{T}} \overline{H}_{,\mathbf{UU}} \overline{\mathbf{A}}^j \mathbf{U}_h^n n_i \, ds.
\end{aligned} \tag{4.26}$$

Making use of the scalar product

$$\langle \mathbf{V}, \mathbf{W} \rangle_{\overline{H}} = \int_\Omega \overline{\mathbf{V}}^{\mathrm{T}} \overline{H}_{,\mathbf{UU}} \mathbf{W} \, d\mathbf{x} \tag{4.27}$$

and the corresponding norm

$$\|\mathbf{V}\|_{\overline{H}} = (\langle \mathbf{V}, \mathbf{V} \rangle_{\overline{H}})^{1/2}, \tag{4.28}$$

we can rewrite (4.26) as

$$\begin{aligned}
&\lambda \left[\|\mathbf{U}_h^n\|_{\overline{H}}^2 + \Delta t \left\| \left(\frac{\Delta t}{2} + Ch \right) \overline{\mathbf{A}}^i (\mathbf{U}_h^n)_{,i} \right\|_{\overline{H}}^2 \right] \\
&\quad = \|\mathbf{U}_h^n\|_{\overline{H}}^2 + \Delta t \, \langle \mathbf{U}_h^n, \overline{\mathbf{A}} (\mathbf{U}_h^n)_{,i} \rangle_{\overline{H}} \\
&\qquad - \Delta t \int_\Gamma (\overline{\mathbf{U}}_h^n)^{\mathrm{T}} \overline{H}_{,\mathbf{UU}} \overline{\mathbf{A}}^i \mathbf{U}_h^n n_i \, ds.
\end{aligned} \tag{4.29}$$

We observe that

$$\begin{aligned}
&\int_\Omega [(\overline{\mathbf{U}}_h^n)^{\mathrm{T}} \overline{H}_{,\mathbf{UU}} \overline{A}^i \mathbf{U}_h^n]_{,i} \, d\mathbf{x} \\
&\quad = \int (\overline{\mathbf{U}}_h^n)_{,i}^{\mathrm{T}} \overline{H}_{,\mathbf{UU}} \overline{\mathbf{A}}^i \mathbf{U}_h^n \, d\mathbf{x} \\
&\qquad + \int_\Omega (\overline{\mathbf{U}}_h^n)^{\mathrm{T}} \overline{H}_{,\mathbf{UU}} \overline{\mathbf{A}}^i (\mathbf{U}_h^n)_{,i} \, d\mathbf{x} \\
&\quad = \langle \mathbf{U}_h^n, \overline{\mathbf{A}}^i (\mathbf{U}_h^n)_{,i} \rangle_{\overline{H}} + \overline{\langle \mathbf{U}_h^n, \overline{\mathbf{A}}^i (\mathbf{U}_h^n)_{,i} \rangle_{\overline{H}}} \\
&\quad = 2 \Re \langle \mathbf{U}_h^n, \overline{\mathbf{A}}^i (\mathbf{U}_h^n)_{,i} \rangle_{\overline{H}}.
\end{aligned} \tag{4.30}$$

Substituting (4.30) into (4.29), we get

$$\begin{aligned}
&\lambda \left[\|\mathbf{U}_h^n\|_{\overline{H}}^2 + \Delta t \left\| \left(\frac{\Delta t}{2} + Ch \right) \overline{\mathbf{A}}^i (\mathbf{U}_h^n)_{,i} \right\|_{\overline{H}}^2 \right] \\
&\quad = \|\mathbf{U}_h^n\|_{\overline{H}}^2 - \frac{\Delta t}{2} \int_\Gamma (\overline{\mathbf{U}}_h^n)^{\mathrm{T}} \overline{\mathbf{U}}_{,\mathbf{UU}} \overline{\mathbf{A}}^n \mathbf{U}_h^n \, ds \\
&\qquad + i \, \Delta t \Im \langle \mathbf{U}_h^n, \overline{\mathbf{A}}^i (\mathbf{U}_h^n)_{,i} \rangle_{\overline{H}}.
\end{aligned} \tag{4.31}$$

Finally, using the Cauchy–Schwartz inequality

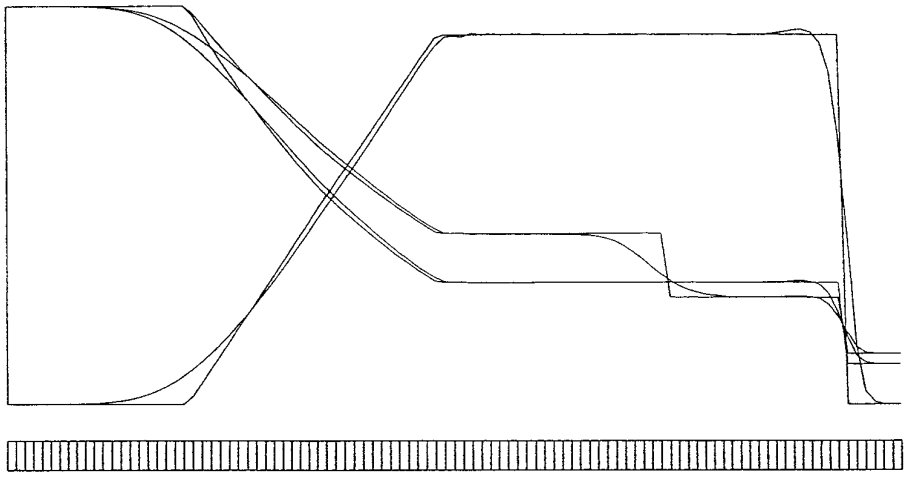

FIG. 3. Shock tube problem: density, velocity, and pressure after 0.25s ($C_0 = 0.3$).

$$(\langle \mathbf{U}_h^n, \overline{\mathbf{A}}^i(\mathbf{U}_h^n)_{,i}\rangle_{\overline{H}})^2 \le \|\mathbf{U}_h^n\|_{\overline{H}}^2 \|\mathbf{A}^i(\mathbf{U}_h^n)_{,i}\|_{\overline{H}}^2 \tag{4.32}$$

we estimate $|\lambda|^2$,

$$|\lambda|^2 \le \frac{(\|\mathbf{U}_h^n\|_{\overline{H}}^2 - (\Delta t/2)\int_\Gamma (\overline{\mathbf{U}}_h^n)^{\mathrm{T}} \overline{H}_{,\mathbf{UU}} \overline{\mathbf{A}}^n \mathbf{U}_h^n \, ds)^2 + (\Delta t)^2 \|\mathbf{U}_h^n\|_{\overline{H}}^2 \|\overline{\mathbf{A}}^i(\mathbf{U}_h^n)_{,i}\|_{\overline{H}}^2}{[\|\mathbf{U}_h^n\|_{\overline{H}}^2 + \Delta t \|(\Delta t/2 + Ch)\overline{\mathbf{A}}^i(\mathbf{U}_h^n)_{,i}\|_{\overline{H}}^2]^2}. \tag{4.33}$$

The result confirms that also at the discrete level we can maintain the stability of solutions if we control the fluxes on the boundary. If the boundary integral vanishes then $|\lambda|^2 \le 1$ and the scheme is *unconditionally stable.*

Discrete Nonlinear Stability Analysis

The result concerning the nonlinear time stability of the implicit Euler scheme can be formally reproduced by substituting in the corresponding variational formulation $\mathbf{W} = H_{,\mathbf{U}}(\mathbf{U}^{n+1})$. This step is impossible at the discrete level, unless $H_{,\mathbf{U}}(\mathbf{U}_h^{n+1})$ belongs to the *discrete* space of test functions $\mathbf{V}_h$. This is guaranteed if the entropy variables are used (see [42] for details). In the general case, only an approximate stability result can be derived by substituting for $\mathbf{W}$ the $\mathbf{V}_h$-interpolant of $H_{,\mathbf{U}}(\mathbf{U}_h^{n+1})$. The resulting error seems to be negligible, however. In particular, in practical calculations, we have never encountered a situation in which the implicit Euler scheme would not lead to the satisfaction of stability inequality (4.16) at the discrete level, i.e., with $\mathbf{U}^{n+1}$ and $\mathbf{U}^n$ replaced with the FE counterparts $\mathbf{U}_h^{n+1}$, $\mathbf{U}_h^n$.

Solution Strategy—Transient Problems

The solution procedure consists in solving a sequence of problems (4.24) with viscous matrices $\mathbf{K}_N^{ij}$ given by (2.6). In addition, at each time step we require that the solution $\mathbf{U}_h^{n+1}$ satisfies the discrete nonlinear stability condition,

$$\int_\Omega H(\mathbf{U}_h^{n+1})\, d\mathbf{x} + \Delta t \int_\Gamma F^i(\mathbf{U}_h^{n+1}) n_i \, ds \le \int_\Omega H(\mathbf{U}_h^n)\, d\mathbf{x}. \tag{4.34}$$

This could always be achieved by iterating towards the solution of the implicit Euler scheme but, since we want to preserve the second-order accuracy offered by the Taylor–Galerkin algorithm, we apply some more sophisticated strategy.

We first notice the similarity of dissipation mechanism provided by the second-order Taylor–Galerkin scheme and artificial viscosity terms. Indeed, we have for the Taylor–Galerkin term,

$$\begin{aligned}(\mathbf{U}_{,i}^{n+1})^{\mathrm{T}} H_{,\mathbf{UU}}^{n+1} \frac{\Delta t}{2} \mathbf{f}_{,\mathbf{U}}^i(\mathbf{U}^{n+1}) \mathbf{f}_{,\mathbf{U}}^j(\mathbf{U}^{n+1}) \mathbf{U}_{,j}^{n+1} \\ = \frac{\Delta t}{2} (\mathbf{U}_{,i}^{n+1})^{\mathrm{T}} (\mathbf{f}_{,\mathbf{U}}^i(\mathbf{U}^{n+1}))^{\mathrm{T}} H_{,\mathbf{UU}}^{n+1} \mathbf{f}_{,\mathbf{U}}^j(\mathbf{U}^{n+1}) \mathbf{U}_{,j}^{n+1} \\ = \frac{\Delta t}{2} (\mathbf{f}^i(\mathbf{U}^{n+1})_{,i})^{\mathrm{T}} H_{,\mathbf{UU}}^{n+1} \mathbf{f}^j(\mathbf{U}^{n+1})_{,j},\end{aligned} \tag{4.35}$$

and for the artificial viscosity term,

$$\begin{aligned}(\mathbf{U}_{,i}^{n+1})^{\mathrm{T}} H_{,\mathbf{UU}}^{n+1} Ch\alpha_N \delta_{ij} \mathbf{I} \mathbf{U}_{,j}^{n+1} \\ = Ch\alpha_N (\mathbf{U}_{,i}^{n+1})^{\mathrm{T}} H_{,\mathbf{UU}}^{n+1} \mathbf{U}_{,i}^{n+1} \\ = Ch(\mathbf{f}^i(\mathbf{U}^{n+1})_{,i})^{\mathrm{T}} H_{,\mathbf{UU}}^{n+1} \mathbf{f}^i(\mathbf{U}^{n+1})_{,i}.\end{aligned} \tag{4.36}$$

Thus, the stability estimate for the Euler implicit scheme (4.18) can be rewritten as

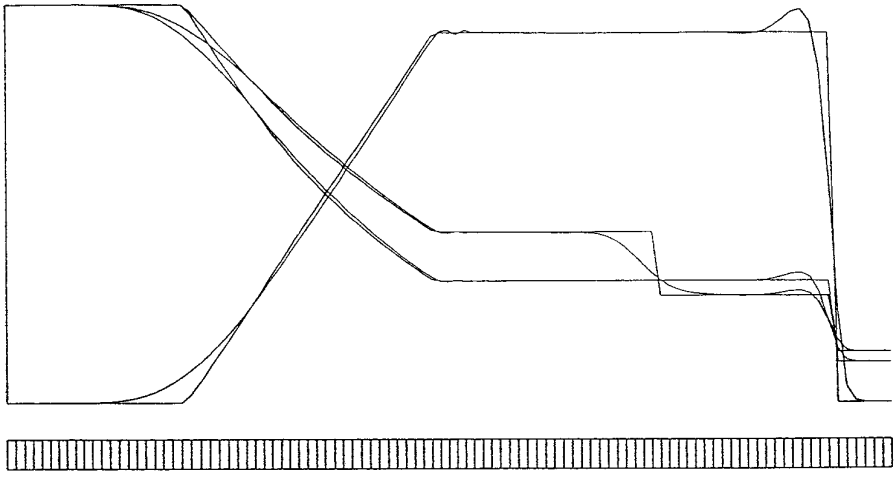

FIG. 4. Shock tube problem: density, velocity, and pressure after 0.25s ($C_0 = 0.2$).

$$\int_\Omega H(\mathbf{U}^{n+1})\,d\mathbf{x} - \int_\Omega H(\mathbf{U}^n)\,d\mathbf{x} + \Delta t \int_\Gamma F^i(\mathbf{U}^{n+1}) n_i\,ds$$
$$\leq -\Delta t \int_\Omega \left(\frac{\Delta t}{2} + Ch\right) (\mathbf{f}^i(\mathbf{U}^{n+1}))^{\mathrm{T}} H^{n+1}_{,\mathbf{UU}} \mathbf{f}^j(\mathbf{U}^{n+1})_{,j}\,d\mathbf{x}$$
$$\leq 0. \tag{4.37}$$

We emphasize that we view (4.37) as a discrete counterpart of the continuous stability estimate (3.4), where the first inequality is replaced with equality sign.

The cost of computations related to the nonlinear stability estimate is negligible, compared with the actual computations. The left-hand side of estimate (4.37) involves calculation of a scalar quantity, and the most expensive part of computations corresponding to the matrix/vector multiplications on the right-hand side of (4.37) is done when evaluating the artificial viscosity terms in the actual solution of the single step problem.

We denote now the left-hand side of (4.37) by $-H_{\mathrm{dis}}$ and

$$\int_\Omega h(\mathbf{f}^i(\mathbf{U}^{n+1}))^{\mathrm{T}} H^{n+1}_{,\mathbf{UU}} \mathbf{f}^j(\mathbf{U}^{n+1})_{,j}\,d\mathbf{x}, \tag{4.38}$$

representing the dissipation due to the artificial viscosity term, by $-H_{\mathrm{vis}}$. When shocks develop and the gradients of the state variables grow, the scheme with too little artificial viscosity becomes unstable. This manifests itself by the growth of H_{vis} not accompanied by decrease of H_{dis}. The loss of stability is related to the appearance of oscillations of the solution near shocks, the defect which can be cured by increasing constant C in front of the artificial viscosity term; we do it until the *increase of* H_{vis} *is accompanied by*

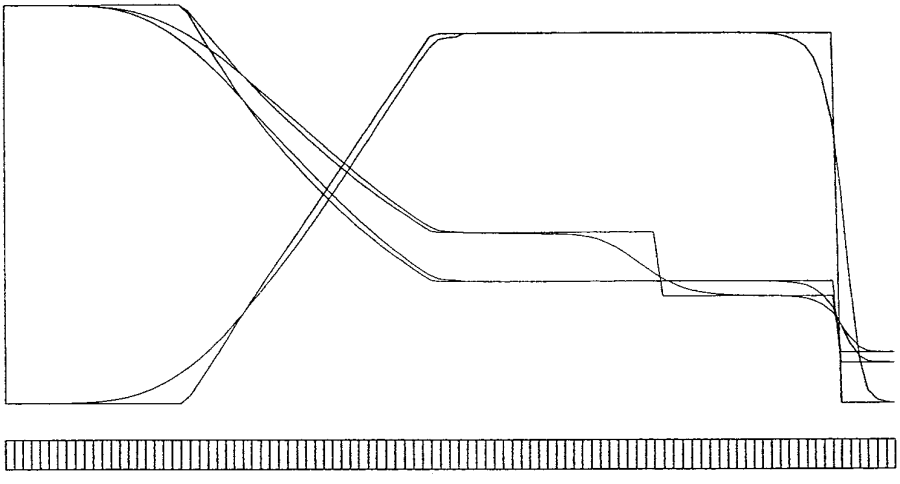

FIG. 5. Shock tube problem: density, velocity, and pressure after 0.25s ($C_0 = 0.4$).

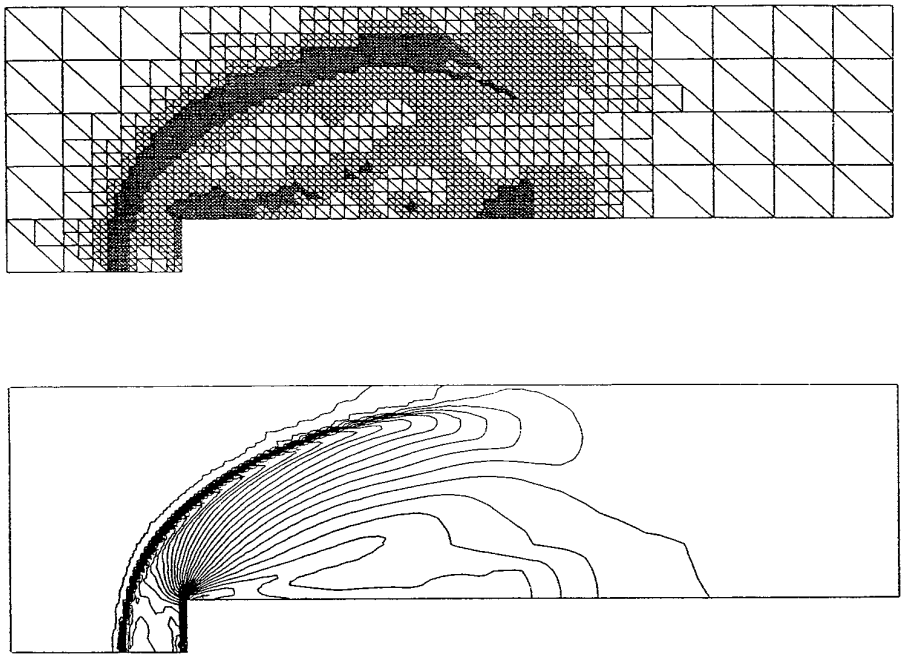

FIG. 6. Channel with a step problem: mesh and density contours after 0.5s.

decrease of H_{dis}. At the same time we always keep H_{dis} nonpositive, resorting to higher values of C if necessary.

In other words, we attempt to monitor not only the sign of H_{dis} which has to stay positive (nonnegative) but also the *time derivatives* of both H_{dis} and H_{vis}, assuring that they have the same sign.

Constant C changes with every time step, starting with some initial value C_0. We always begin with the value for C from the previous time step. If all required conditions are met, we attempt to decrease the value for C, until one of the conditions is violated.

Formally the one-step algorithm looks as follows.

```
Given:  U^n, H_dis(U^n) ≥ 0, H_vis(U^n), C^n, ΔC (an increment
        in C)
        Set: C^{n+1} = C^n, pass = 0
10      solve (4.24) for U^{n+1}
        calculate H_dis(U^{n+1}), H_vis(U^{n+1})
        if (H_dis(U^{n+1}) ≥ 0 and (H_dis(U^{n+1}) − H_dis(U^n))
        (H_vis(U^{n+1}) − H_vis(U^n)) ≥ 0) then
            pass = 1
            C^{n+1} = C^{n+1} − ΔC
            go to 10
        elseif (pass = 0) then
            C^{n+1} = C^{n+1} + ΔC
            go to 10
        else
            return
        endif
```

Solution Strategy— Steady State Problems

We use the transient strategy to iterate towards the steady state solution. In practice, however, as the solution is almost convergent, the optimal constant C oscillates resulting in a periodic-like rather than a steady state solution. In such a situation, we freeze the constant C at some average value and iterate towards the Euler implicit scheme enforcing condition (4.37) only, i.e., making sure that $H_{\text{dis}} \geq 0$.

5. FINITE ELEMENT CODE AND NUMERICAL EXAMPLES

Following a short description of a two-dimensional adaptive code for solving one-step problems (see [33] for details), four numerical examples showing the capabilities of the numerical algorithm developed, are presented.

h-Adaptive Finite Element Code

We describe only the two-dimensional version of the code. The one-dimensional code used in the first example does not utilize h-adaptivity and is conceptually much simpler than the 2D version. The solution strategy in both codes is essentially the same and some characteristic features of the one-dimensional code will be described when considering the first example.

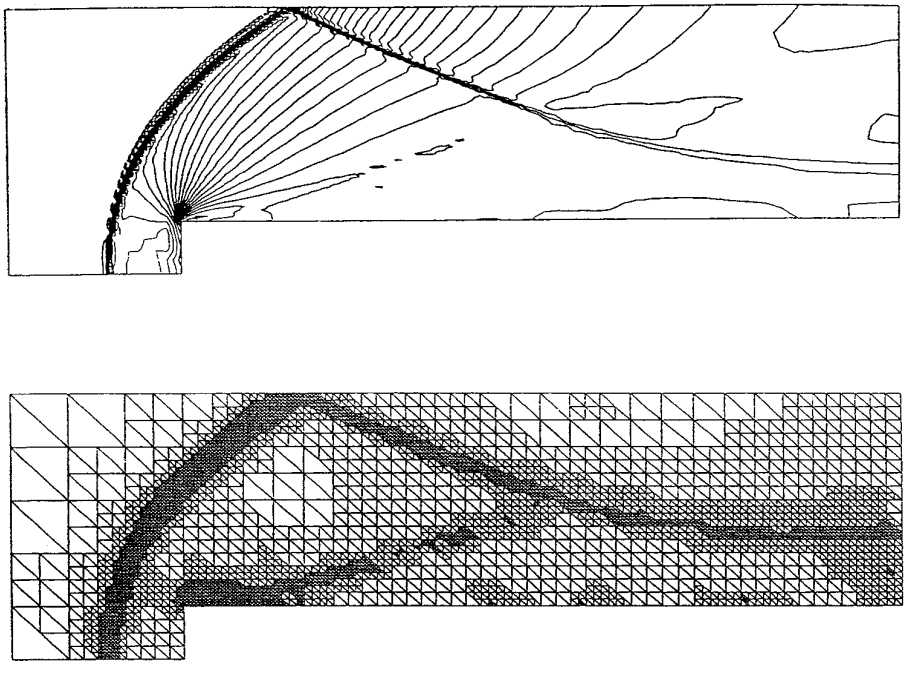

FIG. 7. Channel with a step problem: mesh and density contours after 1.0s.

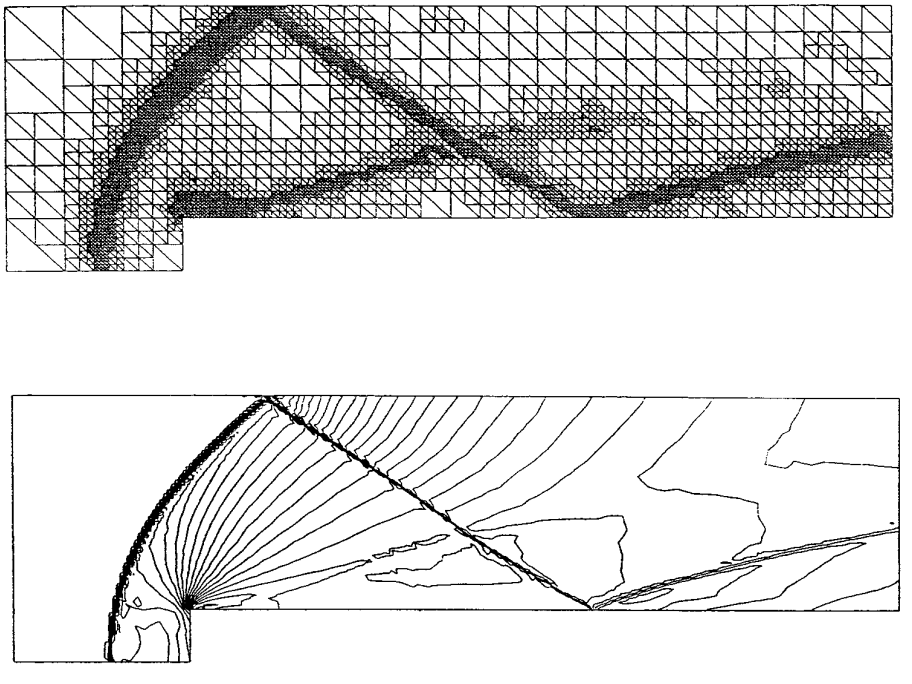

FIG. 8. Channel with a step problem: mesh and density contours after 1.5s.

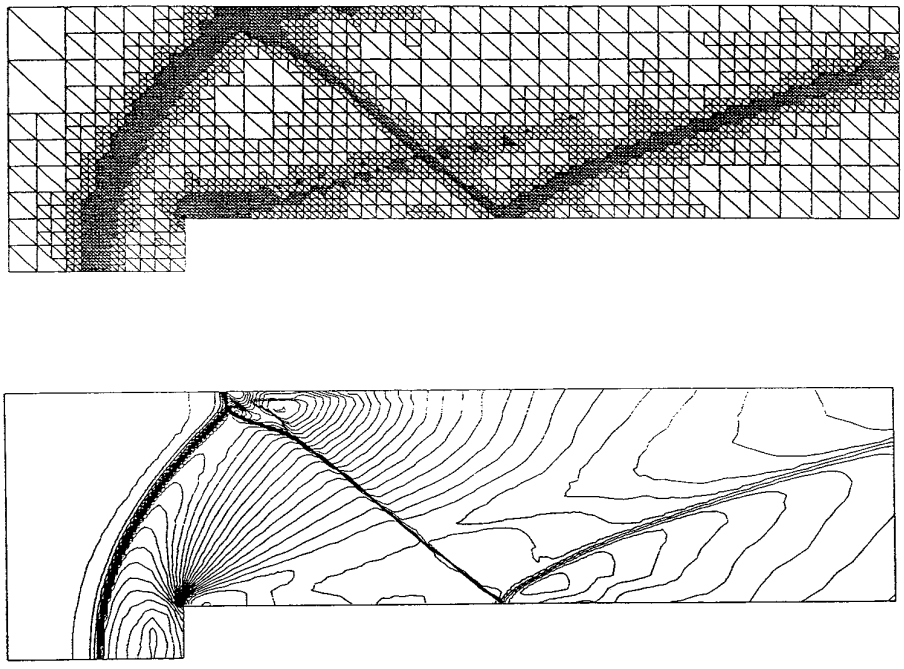

FIG. 9. Channel with a step problem: mesh and density contours after 2.0s.

Domain Discretization and Adaptivity

The two-dimensional computational domain is discretized by using triangular elements. In each element we use linear shape functions and a three-point Gaussian integration quadrature. Each one-step computations constitute a separate problem and may be solved on a different mesh, taking the interpolated result of the previous time step as the initial condition. Between subsequent time steps we perform h-adaptation of the mesh to better resolve the flow features near shocks. As the refinement or unrefinement indicator we use the term:

$$\mathbf{f}^i_{,i} H_{,\mathbf{UU}} \mathbf{f}^j_{,j}. \tag{5.1}$$

This term is based on the residual of the steady state Euler equations $\mathbf{f}^i_{,i}$. For transient computations a large value of $\mathbf{f}^i_{,i}$ indicates regions with fast changes of solution values ($\mathbf{U}_{,t}$ large), and shocks belong surely to such regions. For steady state calculations, the residual $\mathbf{f}^i_{,i}$ is closely related to the error of the finite element approximation. For linear steady state hyperbolic problems, it is even possible to construct a reliable a posteriori error estimates based on $\mathbf{f}^i_{,i}$ [28]. Following the results from the paper cited above, we define for each element, the error indicator

$$I_{\mathrm{el}} = h^2 \mathbf{f}^i_{,i} H_{,\mathbf{UU}} \mathbf{f}^j_{,j}, \tag{5.2}$$

where h denotes a typical dimension of the element, I_{el} is computed in the middle of the element, and h^2 approximates the integration over the element. Observe that for h decreasing, I_{el} decreases as well and, assuming that the link between the error of approximation and I_{el} is maintained for nonlinear problems as well, the overall error will diminish. The actual adaptation strategy is simple. If I_{el} exceeds some limit value then the corresponding element is refined. We use only one technique—the division of the triangle into four pieces (see, e.g., Fig. 6 for the example of a refined mesh). One-irregular meshes are allowed (the vertices of refined elements may lie in the middle of the sides of bigger elements), and the methodology of constrained approximation [32] is applied. The four elements resulting from the division of one element are unrefined back into one if the sum of their error indicators is less then some limit value. Thanks to this procedure, the refined region follows the shocks (and other regions detected by the indicator).

Boundary Conditions

The natural (Neumann) boundary conditions imposed on derivatives of solution components are naturally incorporated into the variational, finite element formulation. The essential (Dirichlet) boundary conditions imposed on the values of solution components are enforced by means of the penalty method. This can be done by adding the terms

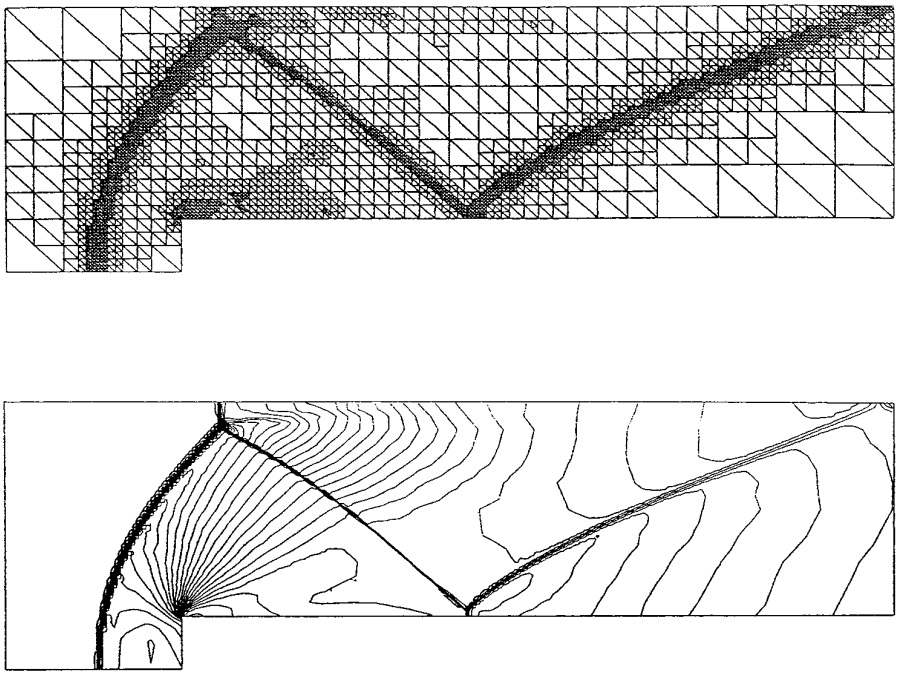

FIG. 10. Channel with a step problem: mesh and density contours after 2.5s.

$$\int_{\Gamma^{\text{in}}} \frac{1}{\varepsilon} \mathbf{W}_h^{\mathrm{T}} \mathbf{U}_h^{n+1}\, dS \tag{5.3}$$

and

$$\int_{\Gamma^w} \frac{1}{\varepsilon} [(\mathbf{W}_h)_2 n_1 + (\mathbf{W}_h)_3 n_2]([\mathbf{U}_h^{n+1})_2 n_1 + (\mathbf{U}_h^{n+1})_3 n_2]\, dS \tag{5.4}$$

to the left-hand side of (4.24) and the term

$$\int_{\Gamma^{\text{in}}} \frac{1}{\varepsilon} \mathbf{W}_h^{\mathrm{T}} \mathbf{U}_h^{B}\, dS \tag{5.5}$$

to the right-hand side of (4.24), where ε is a small penalty parameter and $\mathbf{U}_h^B$ is an interpolant of the continuous boundary condition on the finite element mesh. When transformed into the system of equations, the initial form of the boundary conditions, $\mathbf{U}_h^{n+1} = \mathbf{U}_h^B$ on Γ^{in} and $u_n = 0$ on Γ^w is recovered within the error of order ε. When dealing with boundary conditions enforced by the penalty method, one has to keep in mind that the finite element domain is a polygon, while domains of continuous problems may be smooth. This difficulty can be overcome by considering the penalty method pointwise. Formally this can be achieved also by exchanging the standard Gaussian integration with the two-point Gauss–Lobatto quadratures and, additionally, for the terms with the normal direction involved, by uniquely defining the unit outward normal at each integration point (in case of corners this can be achieved by taking the average of unit vectors normal to two adjacent sides).

Solution of System of Linear Equations

The standard finite element procedures applied to the variational formulation (4.24) lead to a system of linear algebraic equations which is solved by a frontal or an iterative solver. In order to avoid the problems with ill-conditioning of the system, the two parameters Δt and h are chosen to have the same order. Since the algorithm is implicit (implying unconditional stability for linear problems), we do not have to comply with any CFL-like condition, typical for explicit methods. For the Euler and the Navier–Stokes equations, the analog of the CFL condition contains the biggest eigenvalue $\max\{\lambda_p\}$ of the Euler Jacobian matrix $\mathbf{f}^i_{,\mathbf{U}}$. For nonuniform meshes, we speak about the global CFL number being the biggest of the element CFL numbers:

$$\mathrm{CFL} = \max_{\text{el}} \mathrm{CFL}_{\text{el}}, \quad \mathrm{CFL}_{\text{el}} = \frac{h}{\Delta t \max\{\lambda_p\}}, \tag{5.6}$$

where h is the element dimension. In numerical examples we have used time steps and meshes resulting in the element CFL numbers ranging from 0.1 to 2. The last number corresponds to the case where very fine meshes were used

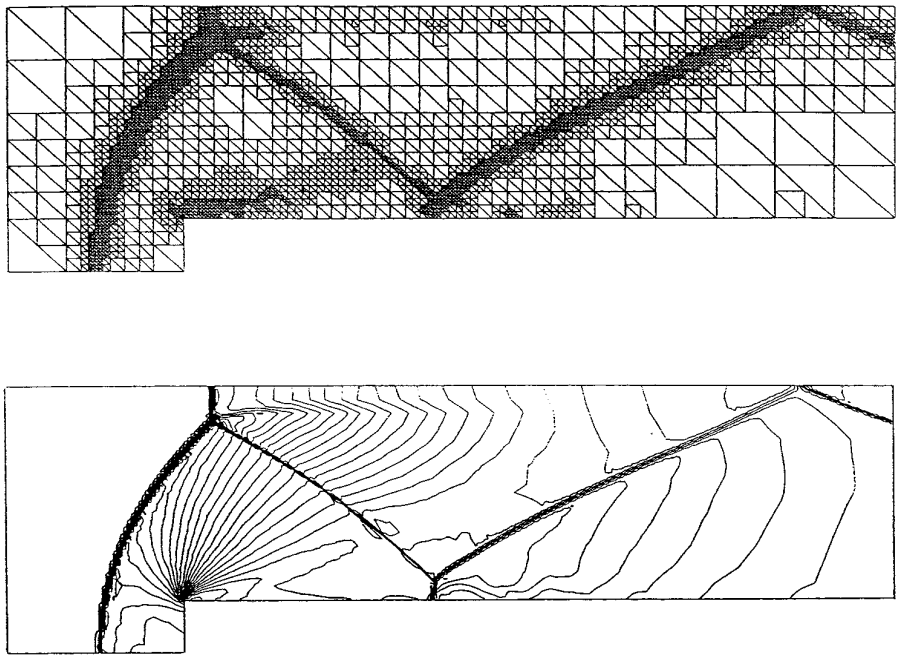

FIG. 11. Channel with a step problem: mesh and density contours after 3.0s.

and the choice of a smaller time step would slow down the solution procedure.

Selection of an Initial Value for the Dissipation Constant

The mechanisms of the entropy dissipation by the Taylor–Galerkin and artificial viscosity terms are very similar. This prompted us to select the initial values of constant C in the simulations in such a way that both terms would contribute with roughly the same amounts of the dissipated entropy. This, rather ad hoc, procedure corresponds to the usual practice in the FE simulations. All values used in the computations are specified subsequently in the text.

Numerical Examples

All computations presented in this subsection were performed on a desktop workstation (2.3 MFlops, 16MB RAM). In all examples ratio of specific heats was assumed to be 1.4 (the theoretical value for biatomic gases widely accepted for the air).

Transient Problems

SHOCK TUBE PROBLEM. The well-known shock tube problem (the classical Riemann problem) describes changes in the tube (of length 1 for simplicity) filled with a gas which initially stays at rest and has only two states -ρ_L, p_L in the left half of the tube, and ρ_R, p_R in the right half. The main advantage of the problem is that its exact solution is known and it exhibits all the interesting features of the compressible flow: shock, contact discontinuity, and rarefaction wave. In the actual computations we have used the values:

$$\rho_L = 1.0, \quad p_L = 1.0, \quad \rho_R = 0.125, \quad p_R = 0.1. \quad (5.7)$$

Figures 1–3 show the state of the gas in the tube after 0.05s, 0.15s, and 0.25s after the beginning of the motion. The mesh of 100 linear elements with uniform length is shown at the bottom of all graphs and the time step 0.005s was used. Lines with sharp corners correspond to the exact solution while the numerical approximations have the shocks smeared. The initial condition is difficult to handle by the algorithm and the results of computations become sensitive to the initial value of the coefficient C in front of the artificial viscosity term. Figures 1–3 correspond to the initial choice $C_0 = 0.3$ and, for comparison, Figs. 4 and 5 show the results after 2.5s for the initial choice $C_0 = 0.2$ and $C_0 = 0.4$. The final value of the coefficient C and the entropy dissipation for the three cases are as follows:

$$\begin{aligned} &C_0 = 0.2, \quad C_{\text{final}} = 0.15, \quad H_{\text{dis}} = 1.3 \times 10^{-2} \\ &C_0 = 0.3, \quad C_{\text{final}} = 0.20, \quad H_{\text{dis}} = 1.5 \times 10^{-2} \\ &C_0 = 0.4, \quad C_{\text{final}} = 0.27, \quad H_{\text{dis}} = 1.6 \times 10^{-2}, \end{aligned} \quad (5.8)$$

It turns out that the actual maximum of the entropy dissipation possible to obtain by controlling C depends on the history of the solution procedure. So the choice of the

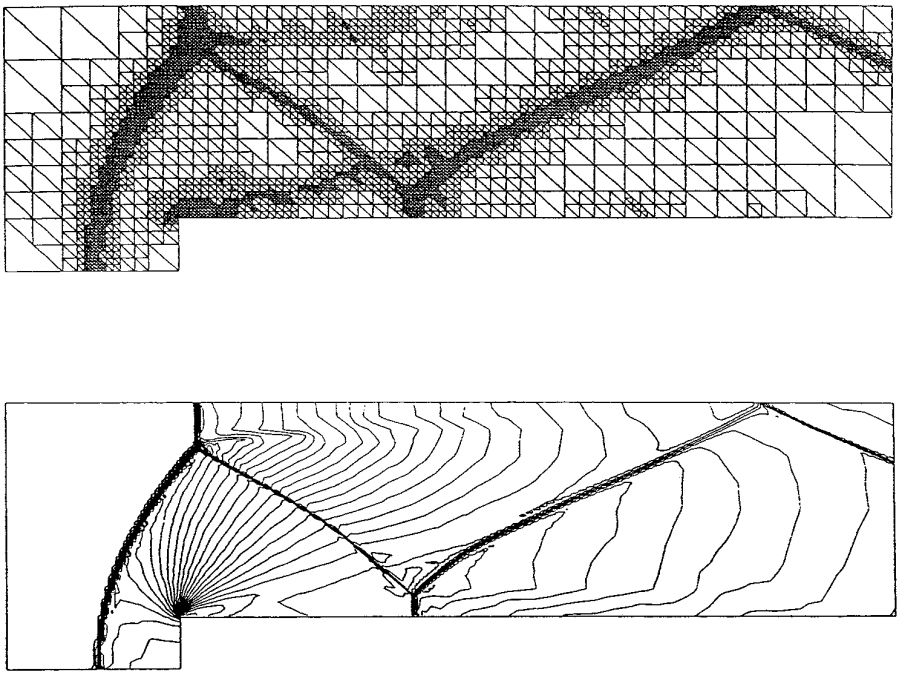

FIG. 12. Channel with a step problem: mesh and density contours after 3.5s.

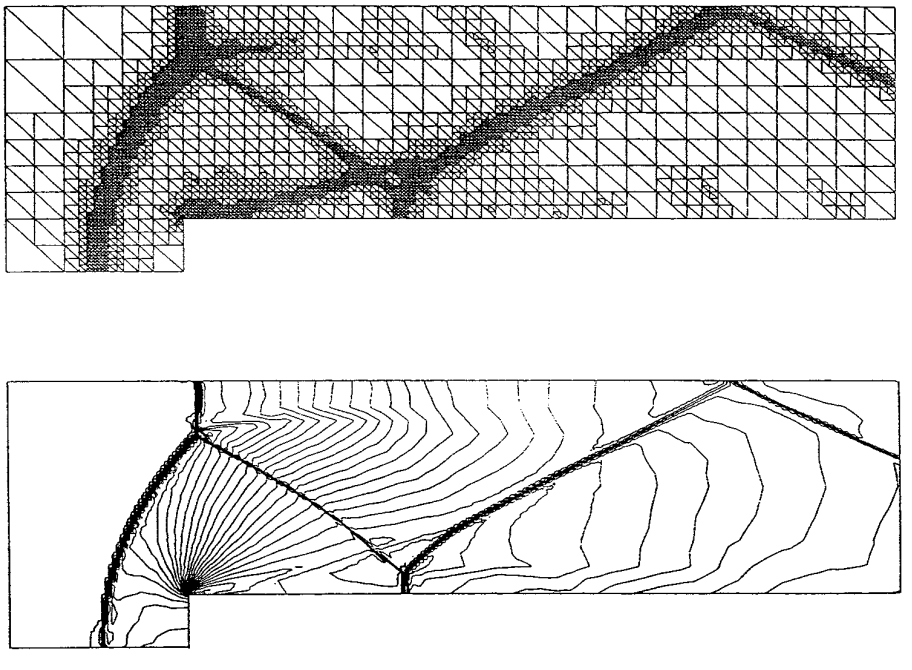

FIG. 13. Channel with a step problem: mesh and density contours after 4.0s.

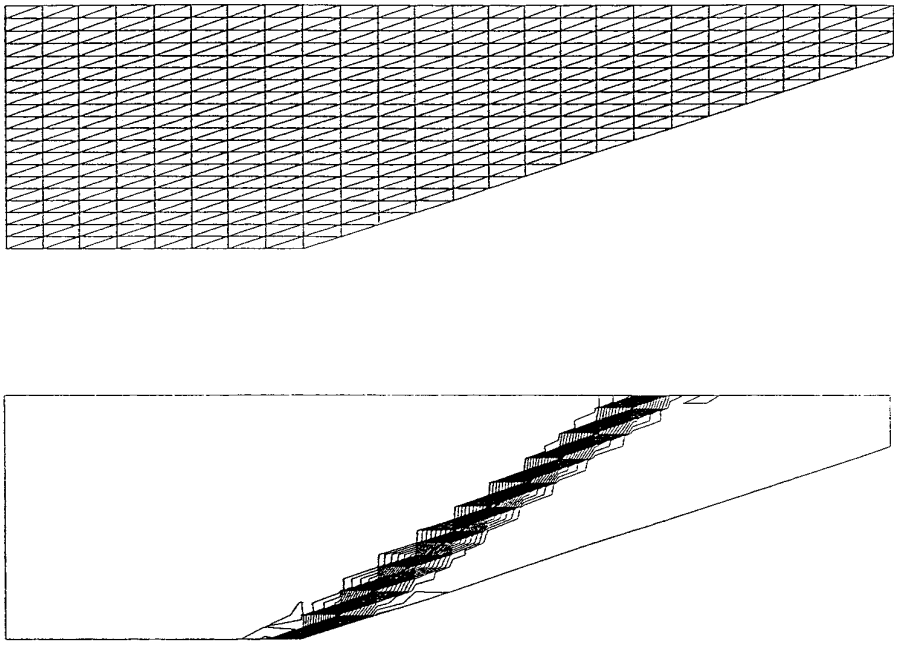

FIG. 14. Wedge problem: mesh and density contours for uniform mesh computations.

initial condition and the initial value of C become important ingredients of the solution strategy.

MACH 3 FLOW IN A CHANNEL WITH STEP. This example is widely used as the benchmark problem for two-dimensional codes in computational fluid dynamics [52]. The initial Mach 3 ($M_\infty = 3$) flow in a channel of length 3 and height 1 is suddenly disturbed by the imposition of the step with height 0.2 at the distance 0.6 from the beginning of the channel (i.e., the computational domain). The standard boundary conditions are imposed. The left-hand side vertical boundary of the computational domain is in the inflow part with the initial values

$$\rho = 1.4, \quad p = 1.0, \quad u_1 = 3.0, \quad u_2 = 0.0, \qquad (5.9)$$

which are kept constant during computations. The right vertical boundary is the outflow boundary and the rest of the boundaries are solid walls. The time step is constant and equal to 0.005 s, resulting in the maximal CFL number close to 2. The mesh adaptation was performed every 10 steps with the limiting value for the indicator I_{el} equal to 0.01 and a limit imposed on the minimal size of the element. Figures 6–13 show the meshes and density contours (30 contours of equal distance) for the time instants from 0.5s to 4s with the interval 0.5s. The constant C was dynamically changed with its initial value 0.4 and the range during the overall computation between 0.1 and 1. This demonstrates the importance of an adaptive change of C to maintain the stability of the algorithm.

Steady State Problems

The commonly used practice of solving steady state problems is to use some transient algorithm expecting that it will provide the quickest path to a steady state solution. In adaptive codes the subsequent mesh adaptations are performed when the solution on the actual mesh converges. We combine the two above approaches with our strategy of controlling the entropy dissipation. Contrary to the transient strategy, there are only few mesh refinements, each one decreasing the minimal element size. At each level of mesh refinement, the transient algorithm with the variable C is used first, and then, after choosing some optimal constant C_{opt}, further computations are performed.

WEDGE PROBLEM. This simple problem consists of a creation of an oblique shock when a Mach 3 flow meets the wall having an angle of 30° with the flow direction. The left vertical boundary is the inflow boundary, the upper and the right boundaries are the outflow boundaries, the bottom part is the symmetry boundary and the sloped boundary is the solid wall. The exact position of the shock is shown in Fig. 14. The following ratios of the state variables on both sides of the shock are the exact values:

$$\frac{\rho_{\text{right}}}{\rho_{\text{left}}} = 2.418; \quad \frac{p_{\text{right}}}{p_{\text{left}}} = 3.771. \qquad (5.10)$$

The meshes and corresponding numerical results are shown in Figs. 14 and 15. The following parameters were

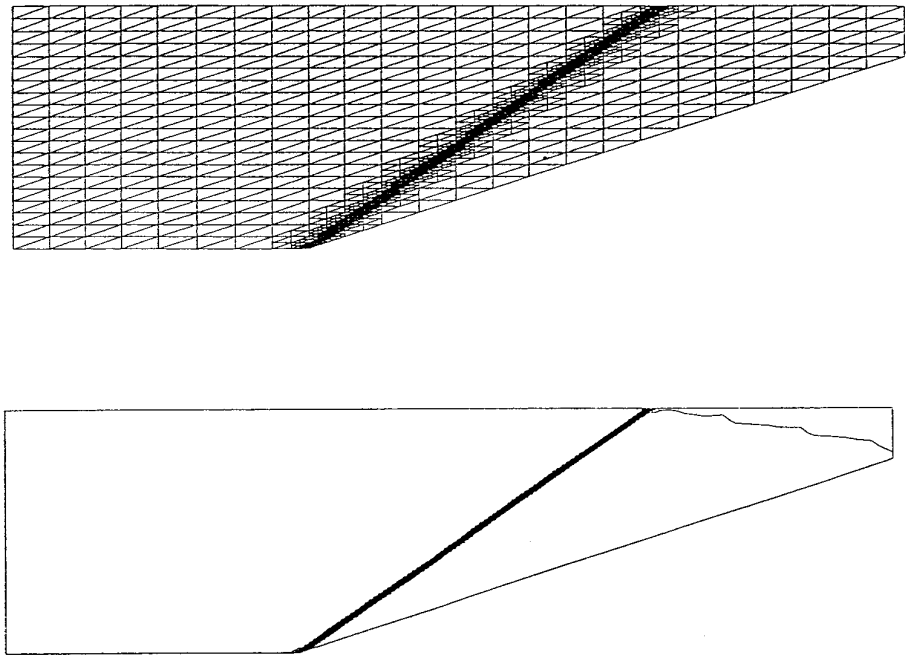

FIG. 15. Wedge problem: mesh and density contours for adaptive mesh computations.

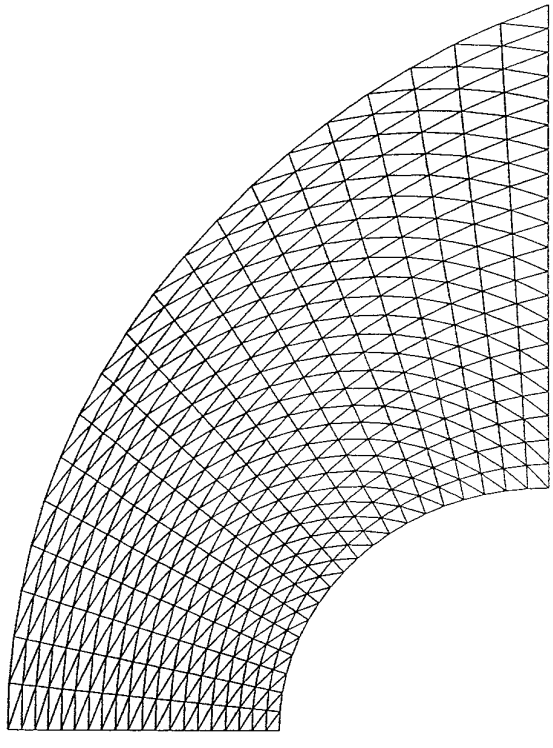

FIG. 16. Blunt body problem: uniform mesh.

used to solve the problem: $CFL_{max} = 0.8$, $C_0 = 0.2$. For refined meshes the constant time step 0.0015s was used resulting in CFL_{max} close to 2. Thirty equidistributed density contours for density are presented. Figure 14 corresponds to the initial mesh with the solution obtained after 150 time steps with the error around 10^{-3} (as the error measure, the maximal difference between the two values of the same solution component at the two consecutive time steps and at the same nodal point was taken). The strong influence of the direction of the shock with respect to the position of elements sides is visible. The error of obtained ratios of state variables (computed far from the shock) with respect to the exact values was less than 1%. The mesh and density contours obtained after three consecutive refinements are shown in Fig. 15. The oscillations of solution appeared when the error fell below 10^{-3}. The final values of state variables, far from the shock, were accurate to five digits.

BLUNT BODY PROBLEM. The last problem is the Mach 6 flow around a circle. The boundary conditions are the same as for the wedge problem with the straight wall replaced by a curved one and the upper boundary being the inflow boundary. The CFL_{max} number 0.8 is used and C_0 is set to 0.2. The results presented in Figs. 16–20 follow the same pattern as for the wedge problem (initial and refined meshes plus corresponding density contours). Figure 19 shows density contours after the transient phase of

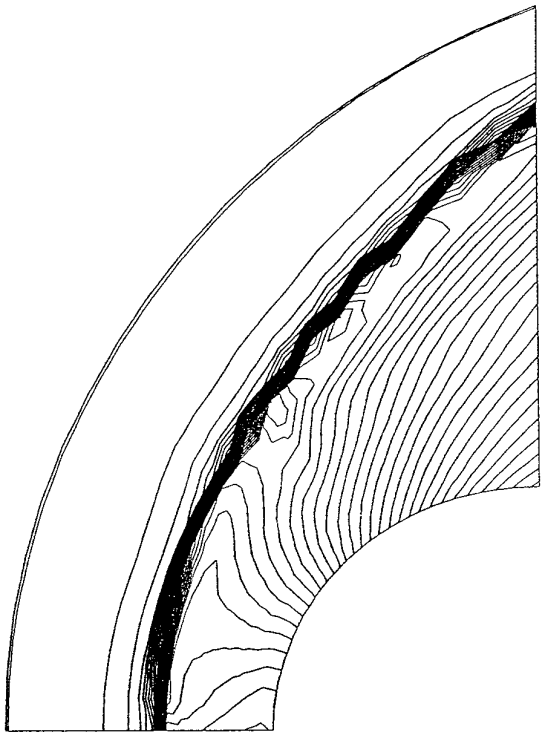

FIG. 17. Blunt body problem: density contours for uniform mesh computations.

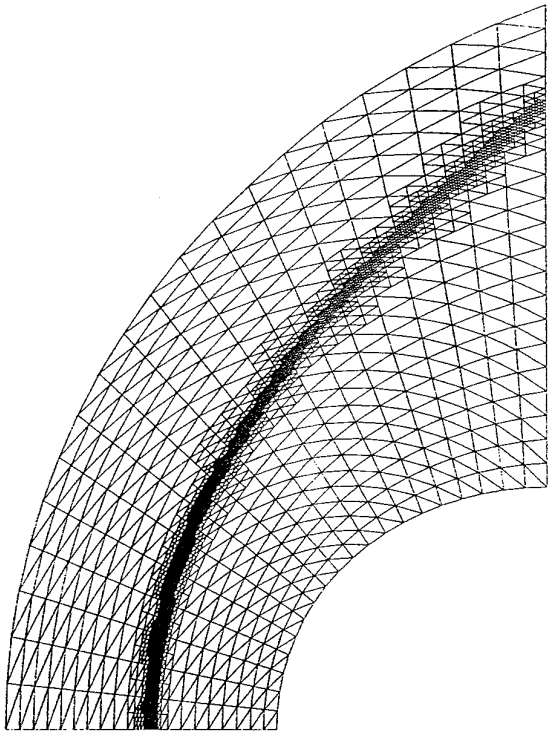

FIG. 18. Blunt body problem: adapted mesh.

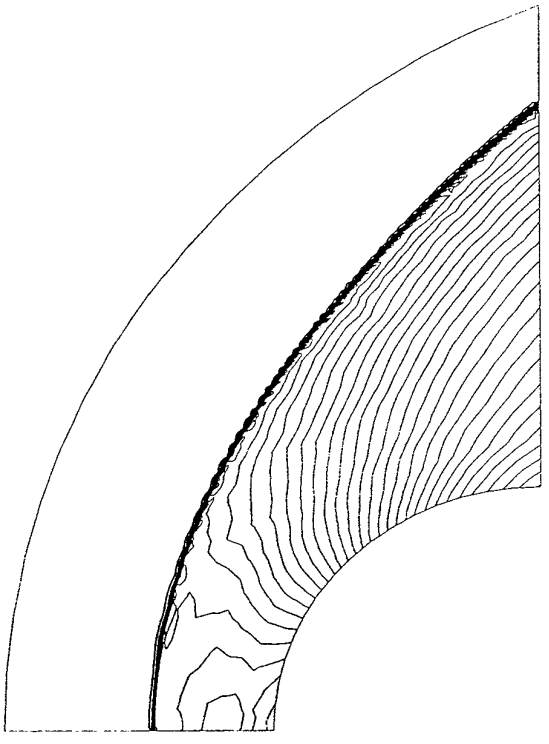

FIG. 19. Blunt body problem: density contours after transient phase.

the algorithm (variable C) while Fig. 20 shows the final result.

6. CONCLUSIONS

In the present work, a new methodology for controlling an optimal amount of artificial dissipation in finite element simulations of compressible gas flows has been presented. The principal idea consists in enforcing a discrete counterpart of the global (over the entire domain) entropy dissipation inequality by adaptively controlling a global coefficient in front of the artificial viscosity term, otherwise assumed usually in an ad-hoc manner. The idea has been successfully verified in practical computations using the Taylor–Galerkin method combined with Johnson and Hughes artificial viscosity model. Finally we emphasize that the entropy dissipation inequality can be interpreted as a nonlinear stability result in terms of the modified entropy function.

Several problems remain to be investigated, to mention a few:

- the entropy dissipation inequality may be enforced on an element level rather than globally, allowing thus to vary the coefficient of artifficial dissipation elementwise,
- a weak, distributional form of the entropy dissipation inequality can be used in place of the integral form,

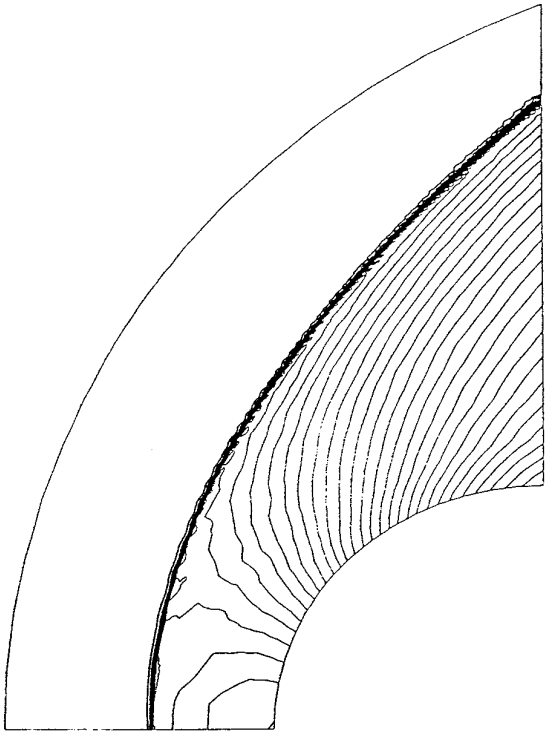

FIG. 20. Blunt body problem: final density contours on adapted mesh.

• higher order approximations, both in time and space variables, should be tried.

We hope to report on these and other related issues in a forthcoming work.

ACKNOWLEDGMENT

The work has been supported by the Polish National Science Foundation (Komitet Badań Naukowych) under Contract 1548/3/91.

REFERENCES

1. J. Glimm, *Commun. Pure Appl. Math.* **18,** 697 (1965).
2. M. G. Crandall and A. Majda, *Math. Comput.* **34,** 1 (1980).
3. J. B. Goodman and R. J. LeVeque, *Math. Comput.* **45,** 15 (1985).
4. R. Sanders, *Math. Comput.* **40,** 91 (1983).
5. A. Harten, *J. Comput. Phys.* **49,** 357 (1983).
6. J. P. Boris and D. L. Book, *J. Comput. Phys.* **11,** 38 (1973).
7. S. T. Zalesak, *J. Comput. Phys.* **31,** 335 (1979).
8. S. Chakravarthy and S. Osher, "High Resolution Application of the Osher Upwind Scheme for the Euler Equations," in *AIAA 6th Computational Fluid Dynamics Conference, 1983.*
9. P. Sweby, *SIAM J. Numer. Anal.* **21,** 995 (1984).
10. P. L. Roe, Lectures in Appl. Math., Vol. 22 (Am. Math. Soc., Providence, RI, (1985), p. 163.
11. A. Jameson and T. J. Baker, AIAA 84-0093 Paper; in *22nd Aerospace Sciences Meeting, Reno, Nevada, 1984* (unpublished).
12. M. G. Edwards, J. T. Oden, and L. Demkowicz, *SIAM J. Sci. Comput.* **14,** 185 (1993).
13. A. Jameson, T. J. Baker, and N. P. Weatherill, AIAA 86-0103 Paper; in *24th Aerospace Sciences Meeting, Reno, Nevada, 1986* (unpublished).
14. R. Löhner, K. Morgan, and J. Peraire, *Commun. Appl. Numer. Methods* **2,** 141 (1985).
15. R. Löhner, K. Morgan, T. Peraire, and M. Vahdati, *Int. J. Numer. Methods Eng.* **7,** 1093 (1987).
16. T. J. R. Hughes, *Int. J. Numer. Methods Fluids* **7,** 1261 (1987).
17. C. Johnson, A. Szepessy, and P. Hansbo, *Math. Comput.* **54,** 107 (1990).
18. F. Shakib, T. J. R. Hughes, and Z. Jordan, *Comput. Methods Appl. Mech. Eng.*
19. J. Donea, *Int. J. Numer. Methods Eng.* **20,** 101 (1984).
20. R. Löhner, K. Morgan, and O. C. Zienkiewicz, *Int. J. Numer. Methods Fluids* **4,** 1043 (1984).
21. J. T. Oden, P. Devloo, and T. Stroubolis, *Comput. Methods Appl. Mech. Eng.* **59,** 327 (1986).
22. A. Safjan and J. T. Oden, *Comput. Methods Appl. Mech. Eng.* **103,** 187 (1993).
23. L. Demkowicz, J. T. Oden, W. Rachowicz, and O. Hardy, *Comput. Methods Appl. Mech. Eng.* **88,** 363 (1991).
24. L. Demkowicz and W. Rachowicz, *Int. J. Eng. Sci.* **25,** 1259 (1987).
25. L. Demkowicz, J. T. Oden, and W. Rachowicz, *Comput. Methods Appl. Mech. Eng.* **84,** 275 (1990).
26. J. Donea and L. Quartapelle, *Comput. Methods Appl. Mech. Eng.* **95,** 169 (1992).
27. J. T. Oden, L. Demkowicz, W. Rachowicz, and T. A. Westermann, "A Posteriori Error Analysis in Finite Elements: The Element Residual Method for Symmetrizable Problems with Applications to Compressible Euler and Navier–Stokes Equations," in *Reliability in Computational Mechanics, Lakeway, Texas, 1989,* edited by J. T. Oden.
28. P. Hansbo and C. Johnson, *Comput. Methods Appl. Mech. Eng.* **87,** 267 (1991).
29. K. Eriksson and C. Johnson, *Math. Comput.* **60,** 167 (1993).
30. R. Löhner, K. Morgan, and O. C. Zienkiewicz, *Comput. Methods Appl. Mech. Eng.* **51,** 441 (1985).
31. O. C. Zienkiewicz and R. L. Taylor, *The Finite Element Method,* 4th ed., Vol. II (McGraw–Hill, London, 1991).
32. L. Demkowicz, J. T. Oden, W. Rachowicz, and O. Hardy, *Comput. Methods Appl. Mech. Eng.* **77,** 79 (1989).
33. L. Demkowicz, W. Rachowicz, K. Banaś, and J. Kucwaj, Cracow University of Technology, Section of Applied Mathematics, Internal Report 4, 1992 (unpublished).
34. J. Peraire, M. Vahdati, K. Morgan, and O. C. Zienkiewicz, *J. Comput. Phys.* **72,** 449 (1987).
35. J. T. Oden, T. Stroubolis, and P. Devloo, *Int. J. Numer. Methods Eng.* **7,** 1211 (1987).
36. J. T. Oden, L. Demkowicz, T. Liszka, and W. Rachowicz, *Comput. Systems Eng.* **1,** 523 (1990).
37. B. Gustafsson and A. Sudström, *SIAM J. Appl. Math.* **35,** 343 (1978).
38. J. C. Strikwerda, Ph.D. thesis, Department of Mathematics, Stanford University, 1976 (unpublished).
39. J. Nordström, *J. Comput. Phys.* **85,** 210 (1989).
40. H. Kreiss and J. Lorenz, *Initial-Boundary Value Problems and the Navier–Stokes equations* (Academic Press, San Diego, 1989).
41. P. Dutt, *SIAM J. Numer. Anal.* **25,** 245 (1988).

42. L. Demkowicz, ''On the Impact of the Entropy Function in Computational Fluid Dynamics (by Finite Elements), in *Proceedings of the International Conference on Differential Equations,* edited by C. Perellò, C. Simó and J. Solà-Morales (World Scientific, Singapore, 1983).
43. O. A. Ladyzhenskaya, *The Mathematical Theory of Viscous Incompressible Flow* (Gordon & Breach, New York, 1969).
44. R. Teman, *Navier–Stokes Equations* (North Holland, Amsterdam, 1977).
45. J. C. Simo and F. Armero, *Comput. Methods Appl. Mech. Eng.* **11,** 11 (1994); **89,** 141 (1991).
46. T. J. R. Hughes, L. P. Franca, and M. Mallet, *Comput. Methods Appl. Mech. Eng.* **54,** 223 (1986).
47. C. Johnson, *Numerical Solutions of Partial Differential Equations by the Finite Element Method* (Cambridge Univ. Press, Cambridge, 1987).
48. R. Courant and K. O. Friedrichs, *Supersonic Flow and Shock Waves* (Springer-Verlag, New York, 1976).
49. R. J. DiPerna, *Arch. Rat. Mech. Anal.* **82,** 27 (1983).
50. L. Demkowicz and L. Sławik, *ZAMM* **72,** 587 (1992).
51. K. Banaś, Ph.D. dissertation, Institut of Fundamental Technological Research of Polish Academy of Sciences, Warszawa, Świętokrzyska 21, Poland, September 1994; Cracow University of Technology, Section of Applied Mathematics, Internal Report 6 (1993), 31-155 Kraków, Warszawska 24, Poland.
52. P. Woodward and P. Colella, *J. Comput. Phys.* **54,** 115 (1984).